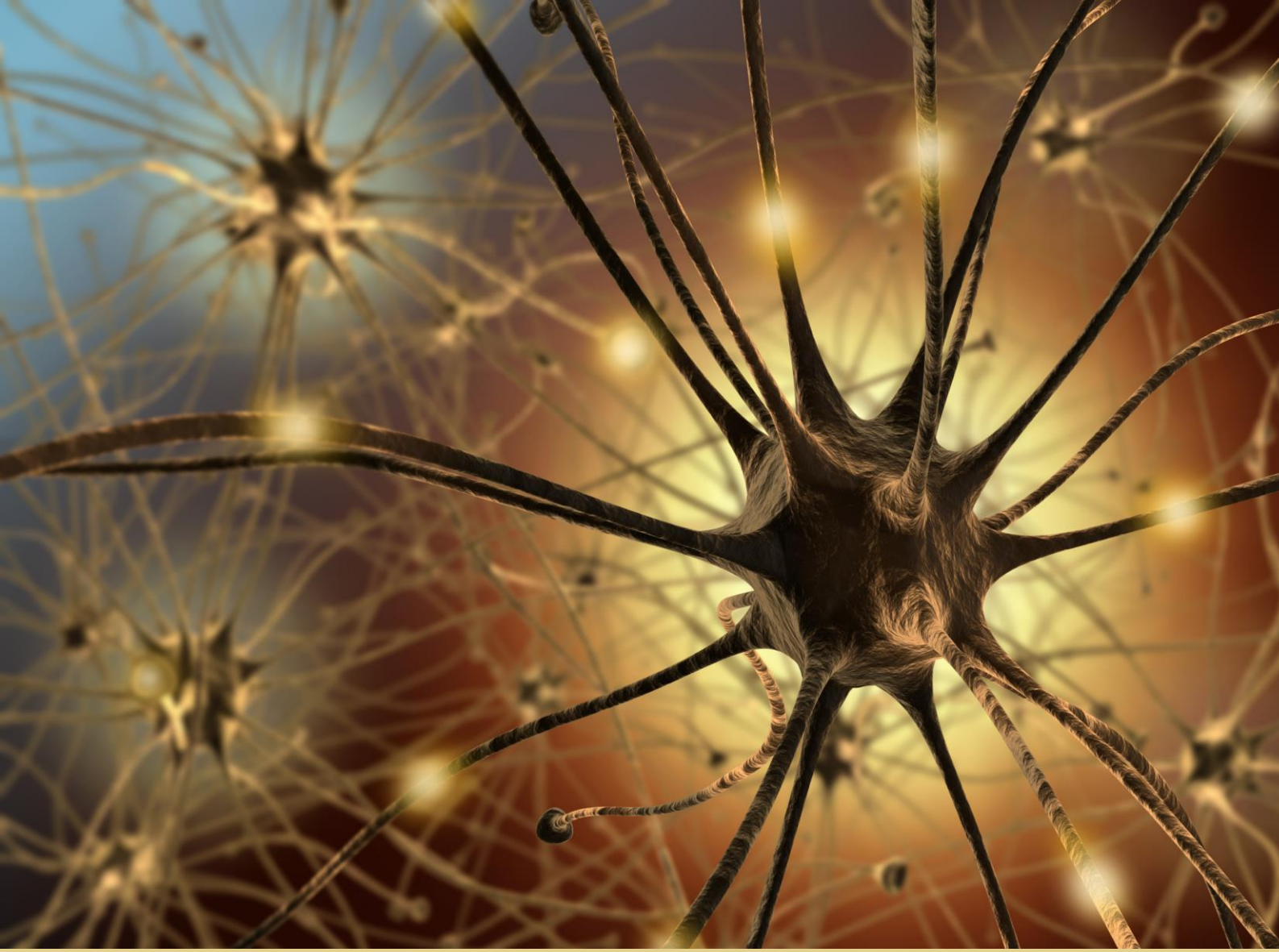

Beatriz Costa Gomes

MODELLING AXONAL GROWTH

Dissertation presented to the University of Coimbra in fulfilment of the requirements necessary for obtaining a M.Sc. degree in Biomedical Engineering

July 2016

· U C ·

UNIVERSIDADE DE COIMBRA

• U C •

FCTUC FACULDADE DE CIÊNCIAS
E TECNOLOGIA
UNIVERSIDADE DE COIMBRA

Beatriz Costa Gomes

Modelling Axonal Growth

Dissertation presented to the University of Coimbra in fulfilment of the requirements necessary for obtaining a MSc degree in Biomedical Engineering.

Supervisors:
Rui Travasso (CFisUC)
Ramiro Almeida (CNC)

Coimbra, 2016

This project was developed in collaboration with:

Centre for Physics of the University of Coimbra (CFisUC)

Center for Neuroscience and Cell Biology (CNC)

Abstract

The axonal growth is an important and complex biological process, essential to the human physiology. Recent discoveries have provided evidences that mRNA translation in neurons occurs not only in the cell body but also in the growth cone, the structure responsible for axon guidance and consequent growth.

The existing mathematical models only touch the surface of this notions and, most of the time, they do not delve into the possible correlation between them. The aim of this project is to enlighten some computational concepts to further explore some of the complexities of axonal growth.

The first presented model is about the 3D morphology changes, namely the protrusions that arise, from mechanical forces originated in the actin filaments, at the growth cone. These *filopodia* search for cues and connect the cell to the surrounding environment.

Later, the 2D model regards the inner workings of the cell: the transport of mRNA from the nucleus to the tip of the axon, which occurs with the help of microtubules, coupled with the neuronal growth dependent on external stimuli.

Although the first model did not have a successful solution, the second is stable and can be a starting foundation to more complex models that are biologically relevant.

Resumo

O crescimento axonal é um processo biológico importante e complexo, essencial para a fisiologia humana. Descobertas recentes demonstraram que a tradução de mRNA em neurónios ocorre não só no corpo celular como também no cone de crescimento, a estrutura responsável pela orientação axonal e seu consequente crescimento.

Os modelos matemáticos actualmente existentes apenas abordam uma pequena parte dos conceitos e, usualmente, negligenciam a possivel correlação entre os mesmos. O objectivo deste projecto é demonstrar alguns conceitos computacionais por forma a poder explorar mais profundamente algumas das complexidades do crescimento axonal.

O primeiro modelo apresentado prende-se com as mudanças morfológicas a 3D, nomeadamente as protrusões, que procuram estímulos exteriores e ligam a célula ao meio que a rodeia, que surgem no cone de crescimento devido a forças mecânicas originadas por filamentos de actina.

Em seguida, o modelo 2D tem em conta o funcionamento interno da célula: o transporte do mRNA do núcleo para a extremidade do axónio, que ocorre com a ajuda de microtúbulos, acoplado ao crescimento neuronal dependente de estímulos externos.

Embora com o primeiro modelo não se tenha conseguido alcançar resultados satisfatórios, o segundo é estável e pode ser um bom ponto de partida para modelos mais complexos e relevantes do ponto de vista biológico.

Contents

Abstract **vii**

Resumo **ix**

1 Introduction **1**
1.1 Biological Background . . . 1
1.1.1 Concepts . . . 1
1.1.2 Diseases and Motivation . . . 5
1.2 Overview of Models . . . 7
1.2.1 Axon Guidance, Growth and Morphology . . . 8
1.2.2 Intracellular Dynamics . . . 9
1.2.3 Composite Models . . . 9

2 Mathematical and Computational Methods **11**
2.1 The Phase-Field Method . . . 11
2.2 3D Shape and Forces Model . . . 12
2.3 2D mRNA Transport Model . . . 16

3 Computational Simulations **19**
3.1 3D Shape and Forces Model . . . 21
3.1.1 Simulation 1 - Bending Energy . . . 23
3.1.2 Simulation 2 - Volume Conservation . . . 23
3.1.3 Simulation 3 - Surface Area Stabilization . . . 27
3.1.4 Simulation 4 - Mechanical Forces . . . 27
3.2 2D mRNA Transport Model . . . 31

4 Conclusions and Future Work **41**

A Mathematical Formulas and Deductions **43**
A.1 Vector Calculus . . . 43
A.2 Useful Mathematical Equalities . . . 43
A.3 Functional Calculus . . . 44
A.4 Dirac's delta function and Heaviside function . . . 44
A.5 3D Shape and Forces Model . . . 45
A.5.1 Deriving ϕ with respect to the space variables . . . 45
A.5.2 Integrating $(\nabla\phi)^2$ . . . 45
A.5.3 Free Energy Functional Calculation . . . 46
A.5.4 Volume and Surface Area Considerations . . . 47
A.6 2D mRNA Transport Model . . . 48

A.6.1 Applying PFM to the mRNA Equations 48
A.7 Euler Method 48
A.8 Mathematical Operators Implementation 48

Bibliography **51**

List of Figures

1.1 Actin dynamics in *filopodia* 2
1.2 Growth cone guidance 4
1.3 mRNA transport into axons 6

2.1 Normal vector 13

3.1 Euler method algorithm flowchart 20
3.2 Initial Condition for the 3D Shape and Forces Model 21
3.3 3D model flowchart 22
3.4 Bending energy: Time evolution of the 3D Shape 23
3.5 Bending energy: Time evolution of Surface Area and Volume 24
3.6 Volume conservation energy: Time evolution of the 3D Shape 25
3.7 Volume conservation energy: Time evolution of Surface Area and Volume . . . 26
3.8 Surface area conservation energy: Time evolution of the 3D Shape 28
3.9 Surface area conservation energy: Time evolution of Surface Area and Volume 29
3.10 Mechanical forces energy: Time evolution of the 3D Shape 30
3.11 2D model flowchart 32
3.12 Initial Condition for the 2D Model 33
3.13 First figure of the 2D Model 34
3.14 Second figure of the 2D Model 35
3.15 Third figure of the 2D Model 36
3.16 Fourth figure of the 2D Model 37
3.17 Fifth figure of the 2D Model 38
3.18 Last figure of the 2D Model 39

List of Tables

3.1 Initial Conditions for the 3D Model Simulations 22
3.2 Constants for the 2D Model Simulations 33

List of Abbreviations

CNS	**C**entral **N**ervous **S**ystem
GC	**G**rowth **C**one
GF	**G**rowth **F**actor
MF	**M**icro**f**ilaments
mRNA	**m**essenger **R**ibo**n**ucleic **A**cid
MT	**M**icro**t**ubules
PDE	**P**artial **D**ifferential **E**quation
PFM	**P**hase-**f**ield **M**ethod
UTR	**U**n**t**ranslated **R**egion

List of Symbols

t	Time Variable
t_{max}	Maximum Time
Δt	Time Increment
Δx	Space Step
ϵ	Interface width
ϕ	Order Parameter

3D Shape and Forces Model

A_i	Ideal Surface Area
A_{old}	Last Iteration Surface Area
E	Total Energy
E_b	Bending Energy
E_f	Mechanical Forces Energy
E_s	Surface Area Conservation Energy
E_v	Volume Conservation Energy
k_1	$\frac{3}{2\sqrt{2}\epsilon^3}$
k_2	$\frac{3}{4\sqrt{2}\epsilon}$
P	Bulk Pressure
V_i	Ideal Volume
V_{old}	Last Iteration Volume
α_s	Surface Area constant
α_v	Volume constant
σ	Surface Tension

2D mRNA Transport Model

D_i	GF Diffusion Constant
G	Growing Factor
k_d	Free mRNA Diffusion Constant
M	Mobility Coefficient
m_f	Free mRNA Concentration
m_l	Linked mRNA Concentration
M_m	Maximum Concentration of linked mRNA
R_{GC}	GC Radius
T	External Growth Factor
$\mathbf{v}$	Microtubule Vector Field
v_{GC}	GC Velocity
v_m	Linked mRNA Velocity

α_p	Growing Rate
α_T	Consumption Rate
β_m	Unbinding Probability
γ	Binding Constant
λ_f	Free mRNA Decay Rate
λ_l	Linked mRNA Decay Rate
ξ	Microtubule Density Function
Φ	$\frac{1+\phi}{2}$
χ	Chemotactic Response of the Membrane

Chapter 1

Introduction

1.1 Biological Background

1.1.1 Concepts

The nervous system is the most complex assembly of organs in the human body. It is responsible for emotions, reactions to external stimuli and defines each person's personality. The nervous system is currently a target of intense investigation. However, a big part of its functionality is still unknown and with the advancement of technology there is an increased but still partial understanding of what happens with its components.

Neurons are the basic unit of the nervous system. They comprise three parts: cell body, dendrites and axon. Although the most commonly known image of these cells is very simple, in reality they present very complex shapes and can be as small as $1\ \mathrm{mm}$ or as large as $1\ \mathrm{m}$. Each cell's shape is usually directly related to its function and neurons are not an exception. As their function is to pass on information to other cells, they are very long so as to reach the extremities of the human body and can be very branched in both dendrites and axon terminals with the intent of establishing communication with a greater number of cells around them. Unlike some other types of cells, neurons maintain their overall shape during the entirety of their lifetime [1].

The intricacies of cell shape are controlled by a cytoskeleton which is, analogously to the entire human body, the skeleton of the cell. This structure has more functions than just structural organization within the cell, but it is also responsible for cellular transport, division and morphology. The three main components of the neuron's cytoskeleton are microtubules, microfilaments and neurofilaments. In this work, we present a detailed view of microtubules, although some concepts regarding microfilaments will also be explained [1].

Microtubules (MT) have a polymer of 50kDa tubulin subunit as the core structure. The protofilaments are composed by α and β tubulin, 13 of which compose a hollow tube. These structures are a critical part of neuronal polarity, as they present a plus and a minus end. In axons, they are organized with the plus end pointing towards the terminal. The polymerization is said to occur in the plus end due to its faster growth regarding the minus end. It's the equilibrium between assembly and disassembly at each end that defines a critical concentration for consistent microtubule growth. Axonal and dendritic MTs are not continuous from the terminals to the cell body but rather dashed-like, nor are they associated with any visible

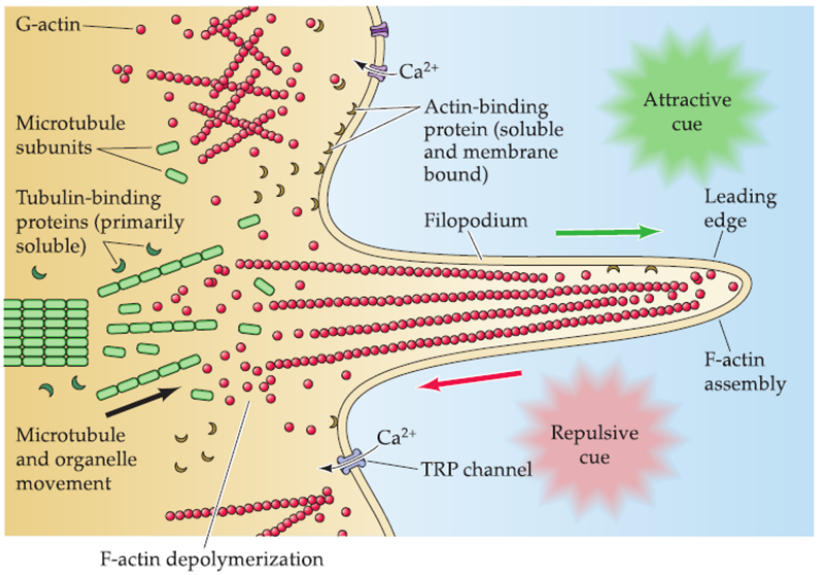

FIGURE 1.1: Distribution and dynamics of cytoskeletal elements in the growth cone. Globular actin (G-actin) can be incorporated into F-actin at the leading edge of the *filopodium* in response to attractive cues. Repulsive cues support the disassembly and retrograde flow of G-actin toward the *lamellapodium*. Organized microtubules make up the cytoskeletal core of the axon, while more broadly dispersed, dynamic microtubules or microtubule subunits are found in apposition to F- and G-actin in the *lamellapodium*. Adapted from [4].

organizing structure such as a MTOC (MT organization centre) [2]. Besides being structural elements, they also act as tracks for organelle and vesicle traffic along axons.

Microfilaments (MF) are actin composed cytoskeleton structures. G-actin monomers form an F-actin polymer. Their concentration increases in developmental structures called neurites, most of which later transform into dendrites while only one of them, assisted by a substructure named growth cone (GC), will make the axon [1].

Axons reach the previously mentioned dimensions by growing at the tip due to the GC, which is composed by two different parts: a smooth region named *lamellapodium* and finger-like regions named *filopodia* [3]. The GC navigates by chemotaxis, i.e., it moves in response to chemical signals in the tissues it grows through. However, since distinct neurons have different functions, they express different receptors at the GCs and can connect to different cells. These structures can respond to signals differently, whether by chemical attraction, repulsion or simply bypassing them. The membrane protrusions appear due to the underlying actin dynamics: the rapid polymerization of actin microfilaments leads to a protrusion, followed by MT elongation and movements to the site (see Figure 1.1). Although MTs do not reach the tip of the GC, they are essential to its progress. Once the GC reaches the target cell, the synapses are formed and the structure disappears.

A very important function of the cytoskeleton, mainly the MTs, is the aforementioned axonal transport. It can be anterograde or retrograde, respectively from the cell body to the axon terminal and reverse. The transport happens due to the binding of molecular motors

(kinesin, dynein and myosin) to the cytoskeleton and to the cargo, which happens due to their use of ATP hydrolysis energy. The transport can either be fast (i.e. in the case of kinesins that bind vesicles and organelles) or slow (e.g. when cytoskeleton proteins are transported along the so called slow components of cell transport). The rate of the latter process limits both axonal growth and regeneration [1].

An important biological concept to retain is about protein synthesis. It starts with the genetic information stored in the deoxyribonucleic acid, also known as DNA. In the nuclei, this information is partially copied into a slightly different type of molecule, the ribonucleic acid or RNA, through a process known as transcription. These information chains then leave the nuclei. In the cytoplasm, the different types of RNA modulate the synthesis. In this work, we focus on the messenger RNA, or mRNA, which contains the genetic copy of the gene for the wanted protein. It then happens the second step of protein synthesis: the translation. With the help of other molecules, e.g. a two-part ribosome, this strand is translated into a protein: each three nucleobases (basic building blocks of the DNA and RNA) form a codon which is translated into the correspondent aminoacid, the monomer of proteins [5]. However, there are also some portions of the mRNA that are untranslated regions (UTR). These regions can contain important information, e.g. the set amount of time the mRNA is available for translation [6].

It was thought for a long time, with the discovery of all these concepts, that in the axons, the actin dynamics occurred as such: the actin mRNA was translated in the cell body, formed MF and only then the MF sections were transported as polymers to the axon terminals. However, in the past decade, some new evidences enlightened a new theory: local mRNA translation and the theory of decentralization [6]. As neurons can be very long cells, it is most natural that there is some degree of compartmentalization [7]. As the terminals can be far from the cell body, they are easily isolated. The local mRNA translation can explain the fast neuronal response and adaptation to external stimuli [8], such as the *de novo* protein synthesis (synthesis from individual monomers and not from recycling proteins after some degradation) that was previously unknown to occur away from the cell body. Furthermore, it was demonstrated that the attraction between growth cones and neurotrophic factors is heavily blocked by the presence of translation inhibitors [9].

Local mRNA translation appears to be an evolutionarily conserved mechanism that decentralizes genomic information and delegates its control to subcellular compartments. It is a very adaptable mechanism linking extrinsic signals in the surrounding tissues to the functional response of the neuron. It is easy to see the connection between this theory and the development of an axon [10]: the GC reacts to stimuli, eliciting asymmetric localization and translation of β-actin (isoform of actin in the cytoskeleton) mRNA and actin regulators (such as RhoA, associated with cytoskeleton regulation specially in actin fibers formation, and cofilin, which binds actin, disassembling the filaments) on the side closest to the external signal, causing the structure to change direction according to the environment (Figure 1.2).

The translation of the different types of proteins heavily depends on both the chemical

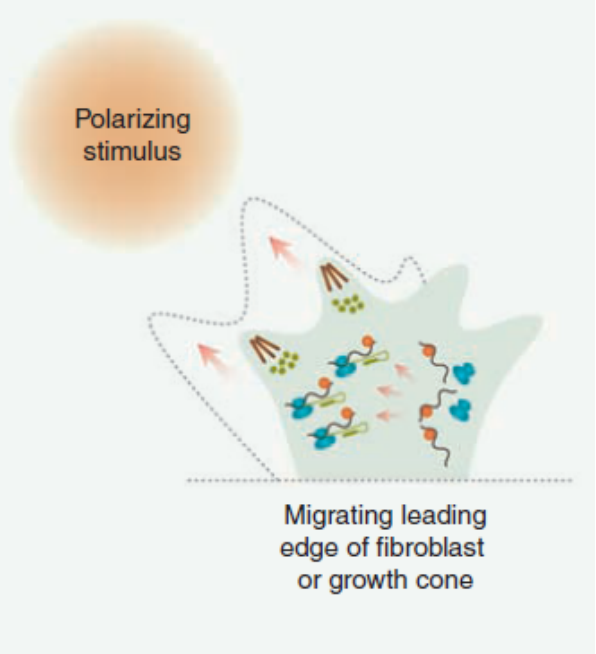

FIGURE 1.2: Growth cone guidance scheme: an external stimuli promotes changes in localization and subcellular translation of mRNA. A polarizing stimulus promotes asymmetrical localization and mRNA translation of β-actin and actin regulators in the region nearest to the stimuli, contributing to the polarized and directional cellular movement. Adapted from [11].

cue present in the environment and the type of receptors in the cell membrane. For example, the mentioned actin mRNA can be triggered by substances like netrin-1 but not by Sema3A [6] and, on the other hand, the regulators (RhoA, cofilin) can be translated in the presence of the latter but not the former. This sustains the theory that different neurons will respond differently to the same surrounding stimulus.

The localization happens after the normal process of the mRNA exiting the nuclei. It is believed that, afterwards, translational repressors silence the mRNA [12], which is later involved by a vesicle, along with other important translational cargo like ribosomes or regulators like RNA-binding proteins (RBP), which recognize specific RNA sequences. These granular bundles are referred to as transport ribonucleoprotein particles (mRNPs) [12].

This new vesicle will then bind molecular motors, usually kinesins even though the bundle can recruit more than one or even change their properties so as to control its own localization. Later, the vesicle will undertake fast transport along the microtubules until they reach the translational site. It is believed that this information is encoded in specific UTRs named zip codes[11]. These sequences also act as translational repressors, which make them essential for the mRNA localization.

Besides the local control of translation in response to external cues, there are several other advantages to this localization: there is an increased local cost effectiveness (production of several copies from the same mRNA strand), it prevents proteins from acting ectopically (i.e.

not in the intended site), facilitates the assembly of macromolecules locally (with the presence of many mRNA strands and the aforementioned cost effectiveness) and presents the properties of newly synthesized proteins [7].

In sum, there are several processes that contribute to the localization: nuclei exportation, localized protection from degradation, polarized active transport mediated by molecular motors and localized anchorage.

1.1.2 Diseases and Motivation

Aging is a process particularly severe to the brain. A lot of degenerative diseases are its direct result and most of them are irreversible. Although the most publicly known pathologies occur in the central nervous system (CNS), mainly in the brain cortex, such as Alzheimer's, Parkinson's or autism, there are others affecting the peripheral counterpart (PNS).

Peripheral neuropathies are a set of diseases affecting neurons and their connection to other tissues, which might impair sensation or movement, depending on the type of neuron affected [3]. There are several types of peripheral disorders, which can be inherited or due to other diseases such as diabetes, autoimmune diseases or infections. Some disorders can be characterized by axonopathy (the dysfunctionality of the axon) while others are predominantly demyelinating. Some of these diseases are characterized by ataxia, a symptom consisting of abnormality in controlling and coordinating movements.

It is important to note that axonal protein synthesis is elicited in response to injury and plays very important roles in axon regeneration and maintenance [13] (see Fig. 1.3), mainly due to the fact that a growth cone is essential for a successful recovery of the injured connections [14]. Moreover, there are new studies indicating that dysfunctional RNA localization and translation represent one of the most common molecular pathologies of neurodevelopmental and neurodegenerative diseases, such as autism (CNS) or ataxias (PNS) [7].

Although recent studies have helped unravel these diseases and advances in a cure for each of them, the available technology and knowledge is still not enough [16]. To quantitatively predict the mechanisms regulating neurons and particularly the axon is a step forward in this direction. If we can understand its process and development, maybe the cure is closer than expected.

Nowadays, experimental biology is not an isolated subject to study diseases, but can be complemented by others. The mathematical modelling and consequent computational counterpart of each process within a cell and also their interconnection is a way to understand how it works with several advantages: it takes less time, less investment and everything can be manipulated much more easily, including parameters that are experimentally impossible to test. Modelling also allows to propose beforehand which parameters are more important

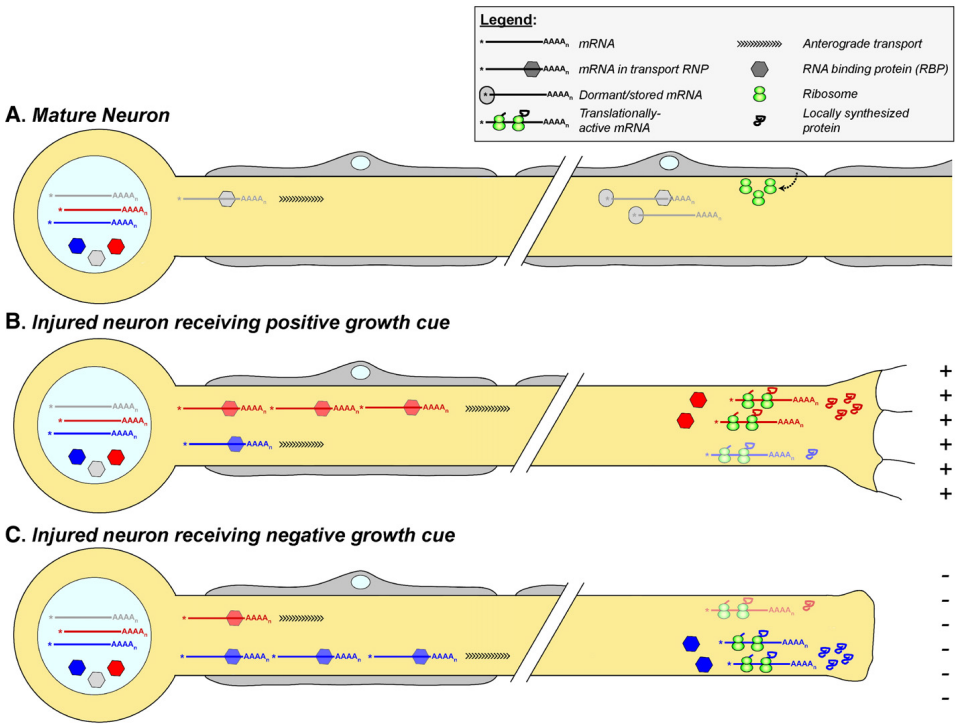

FIGURE 1.3: Transports of mRNAs into axons. Schematic of a PNS neuron in panels A-C with sources of mRNAs and ribosomes indicated by the arrows. Injury of the axon recruits mRNAs into translation helping to initiate the regenerative response [14]. The concentration of mRNA can be from pre-existing (dormant, as seen in **(A)**) or from injury-induced transcriptional events mRNA, according to the external stimuli **(B-C)**. Individual classes of mRNAs and their RBPs are color-coded for transport stimulus: grey = constitutively transported, while the others are transported in response to external growthcues: red = positive and blue = negative. Adapted from [15].

and should be under focus experimentally. So, with the results from the computational calculations we can enlighten the biological model and, in return, biological data can tune the mathematical model, pushing each other forward.

In this work, we propose mathematical ways to model both the actin dynamics in *filopodia* with the associated membrane expansion and the axonal growth and mRNA localization in a neuron, while focusing on a few details, such as the transport of the genetic information to the axon terminal or the advancement of the tip regarding external stimuli.

1.2 Overview of Models

As mentioned in the last section, many of the biological mechanisms involved in axonal growth were only recently discovered. However, as cell biology is a very interesting and rapidly developing area, it was always appealing to mathematical model its intricacies and as such there have been different models presented to explain the different parts of the complexity of a living cell. In this section, some of the main ideas will be explained and the evolution of models throughout the years will be described.

One of the key concepts regarding the modelling for this particular subject is to understand that a neuron is biologically compartmentalized and, as such, can either be represented as an entire cell or as one of its individual components (e.g., the growth cone), and how it not only grows but also polarizes and moves in accordance to external stimuli.

The first step towards modelling the cell is understanding that, mathematically, it represents a region delimited by a frontier: the membrane. However, it is not isolated and maybe influenced by different external stimuli, such as chemical signals. Defining the shape of a cell and how it interacts with the environment will determine its evolution through space and time simulations.

The modelling of a membrane is done by considering it a moving deformable domain. There are four main basic computational techniques to model this problem: the Lagrangian marker method (a simple model which considers the border to be a set of Lagrangian marker points that move according to a given velocity inherent to the problem), the level set method (the boundary is considered to be the level set of a function that describes the distance of any point in the domain from the boundary), phase-field method (considers a order parameter that differs in domains, e.g. inside or outside the cell, with the membrane being the interface between both) and Cellular Potts model (stochastic method that represents the expansion or retraction of the edge of the cell domain) [17].

Most of the mathematical models nowadays regard general ideas or a specific part of the problem. Some are more focused on the axon guidance [18, 19, 20, 21, 22, 23], others on the growth and morphology of the axon [24, 25, 26]. There are a few about the actin dynamics in the process [27], specially inside the *filopodia* [28, 29], while different articles consider the

cargo transport along microtubules and the axon [30, 31, 32]. More recently, there have been some studies considering more than one of these topics and therefore resulting in a more complex model of the biological system [33, 34, 35]. All of these examples will be further explained in the subsections below.

1.2.1 Axon Guidance, Growth and Morphology

As there are many computational approaches to solve biological problems, there are also several mathematical tools which can provide different answers to the existing questions. In this subsection, a brief explanation of some of these paths regarding axonal guidance, growth and morphology will be provided.

Regarding axon guidance, some simple models were developed describing state vectors and concentration of cues in the environment [18] which were later considered as a backbone of the investigation in the field and consequently influencing many other works.

Recently, one of the biggest approaches to this problem has been by considering the axonal growth and guidance as a stochastic problem since it is an event dependent on random variables, as it is nearly impossible to specifically predict where the neurites will appear and later which one will be the axon, or which trajectory the GC will have [19, 20, 21] even if we know where are the chemoattraction and repulsion signals. These models are based on distinct probabilities for each of the events happening while the axon grows and travels through its environment, whether by considering mainly the external cues [20] or the internal response of the GC [19]. More recently, a model has been developed to further explain how the axon guidance happened with an apparent saturation and with so, and comparing to *in vivo* results, found a realistic and precise predictive model of growth cone trajectories [22].

As for computational advances in axonal growth and guidance modelling, for example, there has been software developed, considering the main internal/external mechanisms and environmental elements of the process [23]. Although this software can be useful for rough simulations, it is a very basic view becoming deprecated as new discoveries have been made ever since its development.

The morphology of the axon is not the same throughout the entire process and can be divided into simple stages such as neurite initiation, neurite elongation, axonal guidance and synapse formation in the end [24]. Recently, promising modelling studies have been focused primarily on the GC shape during axon guidance by analysing the set of possible shapes that it can have, and understanding the oscillation of form in axon guidance dynamics [26]. Other computational techniques have been applied to further understand this morphological changes, such as the phase-field method used to understand axonal extensions in cells [25].

1.2.2 Intracellular Dynamics

When approaching a complex subject such as the internal dynamics of a cell, it is necessary to understand that a particular set of reactions will not be isolated from the rest. Therefore, computational and mathematical models usually just recreate the reactions and forces as a whole throughout the cell and not particularly molecule by molecule. For example, considering a phase-field approach in a cell motility model coupled with actin flow, adhesion and morphology [27], the equations depict the *lamellopodium* as a part of the cell with slightly different cytoplasmic characteristics. This is, however, a good example of a model that accurately describes the biological results using a relatively simple set of equations.

There are, however, studies which focus in a smaller part of the cell, namely the *filopodia*. As it has a different actin and microtubule behaviour in comparison with the rest of the cell, the hypothesis about its functioning can be tested using mathematical methods. For example, Naoz *et al.* have been studying and tuning the *filopodia* models throughout the years: firstly, testing the protein localization at the tip by molecular motors and actin threadmilling [28], and later further exploring the role of actin polymerization in the protrusions, elaborating a general model that can explain several morphological features of a *filopodium* [29], such as the protrusion force caused by the actin polymerization and the friction between the consequent actin fiber and underlying cytoplasm.

As aforementioned, neurons are very long and compartimented cells. Therefore, the transport of substances from the cell body to the extremities is a crucial part of their dynamics. Usually, this type of modelling is done resorting to Partial Differential Equations (PDE), solved using numerical integration methods. The models usually consider equations of axonal reaction-diffusion-advection, the three principal components of the dynamics of transported cargo. Zadeh *et al.* [30] presented a consistent model for general cargo transport, along with parameter estimation in accordance to imaging results.

Recently, with the advances in biology regarding mRNA localization, some studies have surfaced considering not only mRNA diffusion throughout the cell body but also advection along the microtubules. These studies were either focused on a more mathematical view of a simple cell, considering microtubules as a vector field and its interaction with the concentration of mRNA, either free or linked [31], or simply by considering the transport of the mRNP [32].

1.2.3 Composite Models

Although the previously mentioned topics have been studied almost independently, more recently there have been emerging mathematical models that connect the two essential parts of the mechanisms.

Najem and Grant [33] developed a phase-field model that coupled both internal actin dynamics and axonal growth. Based on a free energy functional (further explained in the chapter below), they propose a set of equations to model axonal growth, while distinguishing the GC from the rest of the cell as a different phase. However, the limitations of the model, albeit simple, are very hard to overcome as they only managed to model a one-dimensional growth of the cell. More recently, and with a bigger focus in the GC shape, Diehl *et al.* [34] have developed an efficient simulation of tubulin-driven (the monomers of MT) axonal growth, where it is shown that not only the initial growth is fast, but the active transport is more important for velocity than diffusion itself and that the polymerization ratio at the GC does not influence its final shape.

Furthermore, an algorithm was developed to simulate a difficult pathology: axon regeneration after glial scar, which is a phenomenon that happens when there is a CNS injury and glial cells (supporting cells of the nervous system that maintain homeostasis, produce myelin and also protect neurons) form a dense barrier that prevents axons from easily passing by [35]. It is a three-dimensional numerical simulation with a method that handles complicated boundary conditions and allows several different simulations while changing environmental parameters.

Although some of this studies provide a detailed description of a biological process, there is still room for improvement and further investigation may allow new results and ideas to emerge.

Chapter 2

Mathematical and Computational Methods

The main goal in this project is to develop a mathematical model that can successfully simulate in detail the mRNA translation and consequent actin dynamics coupled to axonal growth. However, to do so, two different ideas were pursued: from here onwards named 3D Shape and Forces Model and 2D mRNA Transport Model. The first model is designed to simulate the mechanical forces of a protrusion growth in the cell, along with membrane expansion and the forces produced by the actin filaments. In the second model, the aim is to simulate the axonal transport of both mRNA and proteins (specifically, actin filaments) coupled to the growth itself.

2.1 The Phase-Field Method

Both of the models have the same simulation method behind: the Phase-Field Method (PFM) [36]. The idea is to consider the modelling system as a heterogeneous mixture of two (or more) domains defined by an order parameter, ϕ, that evolves through space and time, and can characterize the change from one phase to the other. This parameter is constant in the bulk of each phase, which interact through a thin frontier. Furthermore, the PFM can be seen as a tool that allows the interface between the phases to evolve according to the simulated model.

Usually, PFM are described by a *free energy functional*, i.e., a function whose input is not a single number but rather an entire function. By the minimization of the functional, the dynamics of the order parameter are controlled by a set of non-linear PDEs. Even for the most complex equation, the integration can be done by simple mathematical methods, such as the time-dependent Euler algorithm. In other words, to solve these types of problems, all equations in the system are written in relation to the order parameter and solved for the entire system with small time steps.

In a real model, the interface thickness ϵ can be really small, approximately $10^{-10}\mathrm{m} = 1\text{Å}$ for mixtures but bigger in case of cell membranes. As for the PFM, the order parameter varies between the absolute values in each phase within a length of small size ϵ. In the limit where

the thickness is close to zero, the PFM dynamics are equivalent to the real results.

The principal idea is to find an expression for the time and space evolution of the order parameter and it can be achieved using the Ginzburg-Landau (or Cahn-Hilliard) free energy functional $E[\phi]$. This expression depends on the entire spacial configuration of the ϕ field. Further considerations of functional calculus can be seen in the Appendix section A.3. This free energy functional implements an energy cost which depends on the interface length, therefore contributing to a minimization of its length.

The order parameters can be regarded as either conserved or non-conserved. If they are conserved, the ϕ equation can be obtained using *Model B*, which considers:

$$\frac{\partial \phi}{\partial t} = \nabla \cdot \left(K \nabla \frac{\delta E}{\delta \phi} \right) \tag{2.1}$$

with K the mobility and E the free energy functional. The main disadvantage of this method is the quadruple derivative than can occur if a Laplacian operator is present in the expression for the functional derivative. The dynamics of non-conserved order parameters, *Model A*, are given by

$$\frac{\partial \phi}{\partial t} = -M \frac{\delta E}{\delta \phi} \tag{2.2}$$

where M is the mobility. In order to preserve the total mass of the system, a Lagrangian multiplier term of the form $\lambda \int \phi(\vec{r}) dV$ can be added to the free energy.

2.2 3D Shape and Forces Model

There are several approaches to model the mechanical forces of actin in the membrane. First, however, it is necessary to find a stable cell membrane model and, more specifically, a three dimensional one. Looking into the existing literature and considering membranes as fluids, red-blood cells can be an example of a good membrane model, since that at equilibrium they present an "unswollen" shape by minimizing their free energy with respect to both surface area and volume, minimizing the integral of the local curvature on the membranes, explained by Canham and later by Helfrich [37]. The Canham-Helfrich energy has been used to simulate different types of cells or vesicles. A phase-field method description of the Canham-Helfrich free energy has also been implemented [38], so this seems a particularly good mathematical model to start with.

The principal idea is to find a stable model for the cell itself [38] and further develop a method by applying mechanical forces to the surface, analogous to how the actin filaments form protrusions in *filopodia* [39].

In the model proposed by Campelo *et al.* [38], the free energy E is proportional to the square curvature of the membrane H: the energy is the same for either a negative or a positive

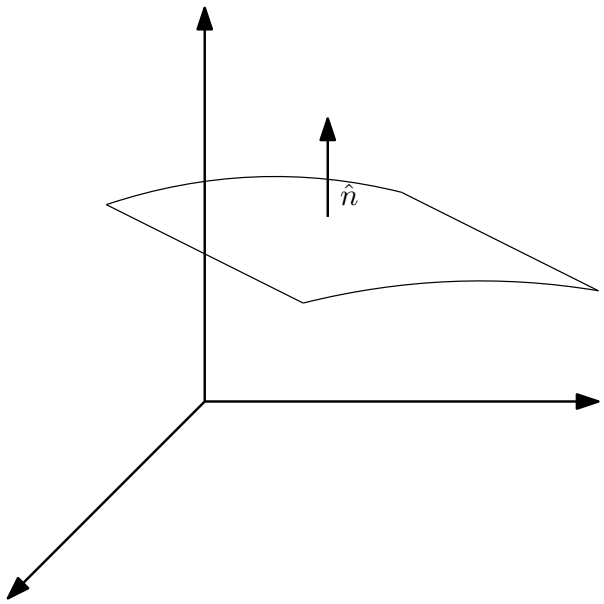

FIGURE 2.1: The normal vector $\hat{n}$ is perpendicular to the surface at a given point.

curvature

$$E = \int H^2 dS. \tag{2.3}$$

The local curvature is described as a variation of the normal vector (Fig. 2.1), $H = \nabla \cdot \hat{n}$.

The backbone of the model presented in this section is initially set in the resulting equation of the minimization of the free energy functional proposed by Campelo *et al.*, which is obtained by setting the phase field function $\psi[\phi]$ to zero:

$$\psi[\phi] = -\phi + \phi^3 - \epsilon^2 \nabla^2 \phi = 0 \tag{2.4}$$

with ϵ being the interface width. In one dimension, the former equation can be simplified to yield

$$\frac{d^2\phi}{dx^2} = \frac{1}{\epsilon^2}\left(-\phi + \phi^3\right) \tag{2.5}$$

which has a tanh-like solution (see Appendix A, equation (A.12)). Substituting $\frac{1}{\epsilon^2} = 2a^2 \Leftrightarrow a = \frac{1}{\sqrt{2}\epsilon}$, the order parameter function can be described as

$$\phi(x) = \tanh\left(\frac{1}{\sqrt{2}\epsilon}x\right). \tag{2.6}$$

However, the goal of this model is to represent the cell in three dimensions. As such, ϕ will be described as a function of the distance $d(\vec{r})$ to the interface

$$\phi(d(\vec{r})) = \tanh\left(\frac{1}{\sqrt{2}\epsilon}d(\vec{r})\right). \tag{2.7}$$

As the distance to the interface is constant (namely, zero) at the said interface, the distance gradient is perpendicular to the surface itself, thus is the same as the normal vector in each

interface point, i.e., $\nabla d(\vec{r}) = \hat{n}$. The curvature can therefore be given as $H = \nabla \cdot \hat{n} = \nabla^2 d(\vec{r})$.

To arrive at a final equation for the curvature, the next step is to derive ϕ with respect to the spatial coordinates, which is further developed in the Appendix section A.5.1. This way, the Laplacian of ϕ is given by:

$$\nabla^2\phi = \frac{1}{\sqrt{2}\epsilon}\left(1-\phi^2\right)\nabla^2 d(\vec{r}) + \frac{1}{\epsilon^2}\left(\nabla \cdot d(\vec{r})\right)^2\left(-\phi+\phi^3\right). \tag{2.8}$$

The first part of this equation has the intended term $\nabla^2 d(\vec{r})$, which can be isolated from the rest. Another important detail is that, as $\nabla \cdot d(\vec{r}) = \hat{n}$, then $\left(\nabla \cdot d(\vec{r})\right)^2 = \hat{n} \cdot \hat{n} = 1$. With all things considered, the expression for the curvature H is

$$\begin{aligned} H = \nabla^2 d(\vec{r}) = \frac{\sqrt{2}\epsilon}{(1-\phi^2)}\left(\nabla^2\phi - \frac{1}{\epsilon^2}\left(-\phi+\phi^3\right)\right) \Leftrightarrow \\ \Leftrightarrow H = \frac{\sqrt{2}}{\epsilon\left(1-\phi^2\right)}\left(\phi - \phi^3 + \epsilon^2\nabla^2\phi\right) \end{aligned} \tag{2.9}$$

which is proportional to the left hand side of the Equation (2.4). The main goal is to use the ϕ field to write the membrane free energy. For this, the Dirac's delta function (see Appendix section A.4) will be used

$$E = \int H^2 \delta\left(\vec{r} - \vec{r}_s\right) dS. \tag{2.10}$$

Since the order parameter function can be considered approximately as a Heaviside function, a good representation of the delta function needed would be:

$$\delta\left(\vec{r} - \vec{r}_s\right) \approx N\left(\nabla\phi\right)^2 = N\left(\frac{\left(1-\phi^2\right)}{\sqrt{2}\epsilon}\nabla \cdot d(\vec{r})\right)^2 = N\frac{\left(1-\phi^2\right)^2}{2\epsilon^2} = \frac{N}{2\epsilon^2}\operatorname{sech}^4\left(\frac{d(\vec{r})}{\sqrt{2}\epsilon}\right) \tag{2.11}$$

where N is a constant and using the fact that $\left(\nabla \cdot d(\vec{r})\right)^2 = 1$. Also, the approximation is valid in the limit where $\epsilon \to 0$. N can be easily determined by normalizing (2.11) (see Appendix A, equation (A.18)). The inverse of the solution of the underlying integral (see Appendix section A.5.2), N, can than be plugged into equation (2.11), resulting in:

$$\delta\left(\vec{r} - \vec{r}_s\right) = \frac{\left(1-\phi^2\right)^2}{2\epsilon^2}\frac{3\epsilon}{2\sqrt{2}} = \left(1-\phi^2\right)^2\frac{3}{4\sqrt{2}\epsilon}. \tag{2.12}$$

Now, the free energy equation can be updated and further developed, as the idea is to have a general model for both bending energy and applied forces

$$\begin{aligned} E \propto \int H^2 \delta\left(\vec{r} - \vec{r}_s\right) d\vec{r} \approx \\ \approx \int \frac{2}{\epsilon^2\left(1-\phi^2\right)^2}\left(\phi - \phi^3 + \epsilon^2\nabla^2\phi\right)^2\left(1-\phi^2\right)^2\frac{3}{4\sqrt{2}\epsilon}d\vec{r} = \\ = \int \frac{3}{2\sqrt{2}\epsilon^3}\left(\phi - \phi^3 + \epsilon^2\nabla^2\phi\right)^2 d\vec{r}. \end{aligned} \tag{2.13}$$

And thus, the free energy of the system is defined by

$$E = \int \frac{3}{2\sqrt{2}\epsilon^3} \left(\phi - \phi^3 + \epsilon^2 \nabla^2 \phi\right)^2 d\vec{r} + \int \frac{3}{4\sqrt{2}\epsilon} \vec{r} \cdot \vec{F} \left(1 - \phi^2\right)^2 d\vec{r}. \tag{2.14}$$

For simplicity, the constant terms of the previous equation will be redefined as $k_1 = \frac{3}{2\sqrt{2}\epsilon^3}$ and $k_2 = \frac{3}{4\sqrt{2}\epsilon}$. The second term reproduces the work exerted on the membrane by a force of density $\vec{F}$.

Although finding an equation for the free energy was the main focus of the mathematical process above, the simulation PFM is applied to the time and space evolution of the order parameter ϕ. As the free energy functional has a Laplace operator, the best way to simulate the system is by using an approximation of *Model A* physics, considering:

$$\frac{\partial \phi}{\partial t} = -\frac{\delta E}{\delta \phi}. \tag{2.15}$$

Using functional calculus (as presented in the Appendix section A.3), it is easier to obtain the intended expression, which will give how much the energy varies if ϕ changes in every point of the space

$$\delta E = \int \frac{\delta E}{\delta \phi} \delta \phi d\vec{r}. \tag{2.16}$$

So far, the free energy expression (2.14) comprises two terms: the bending energy and the applied forces. However, before implementing the external forces to the system, it is necessary to first preserve both volume and surface area as the cell boundary is a stabilized membrane. The final expression will then be composed by four terms:

$$\frac{\delta E}{\delta \phi} = \frac{\delta E_b}{\delta \phi} + \frac{\delta E_f}{\delta \phi} + \frac{\delta E_v}{\delta \phi} + \frac{\delta E_s}{\delta \phi} \tag{2.17}$$

with E_b the bending energy, E_f the applied forces energy, E_v related to the conservation of volume and E_s related to the conservation of surface area. The development of the expressions is further explored in the Appendix section A.5.3. The first two parts of the above equation can be already shown as they have been previously demonstrated in this section, and were deduced in the Appendix equations (A.29) and (A.30) respectively, giving

$$\frac{\delta E_b}{\delta \phi} = 2k_1 \left[\left(\phi - \phi^3 + \epsilon^2 \nabla^2 \phi\right)\left(1 - 3\phi^2\right) + \epsilon^2 \nabla^2 \left(\phi - \phi^3 + \epsilon^2 \nabla^2 \phi\right)\right] \tag{2.18}$$

and

$$\frac{\delta E_f}{\delta \phi} = -4k_2 (\vec{r} \cdot \vec{F}) \left[\left(1 - \phi^2\right)\phi\right]. \tag{2.19}$$

For the conservation of volume, the bulk property needed is the pressure, P. The idea is that for the same pressure, a larger volume will diminish the overall energy. Therefore, if the volume is decreased during the simulation, an increase in pressure can compensate. As for the PFM, to calculate the volume of the structure, one can only consider the order parameter inside the cell, i.e., above the environment value (which, in this case and later explained, will

be $\phi_{outside} = -1$). As such, the energy will be

$$E_v = -P \int \left(\frac{1+\phi}{2} \right)^2 (2-\phi) d\vec{r} \tag{2.20}$$

which guarantees the above conditions as the volume is the sum of all the order parameters of the system that are different from -1, and is negative as ϕ is never greater than 1. After the demonstration of the Appendix equation (A.31), the final expression will be:

$$\frac{\delta E_v}{\delta \phi} = -\frac{3}{4} P \left(1 - \phi^2\right). \tag{2.21}$$

Finally, to achieve surface area stabilization, the essential property is the surface tension σ. As it is a property that will only act on the surface, the simplest way to guarantee it is to apply the delta function previously demonstrated

$$E_s = \sigma \int \delta \left(\vec{r} - \vec{r_s}\right) d\vec{r} = \sigma k_2 \int \left(1 - \phi^2\right)^2 d\vec{r}. \tag{2.22}$$

This only applies to when the order parameter is different from the outside and the inside of the cell, meaning that it will only apply to the surface, as intended. In the Appendix equation (A.32), it is demonstrated how to get the partial derivative needed, obtaining

$$\frac{\delta E_s}{\delta \phi} = -4\sigma k_2 \left[\left(1 - \phi^2\right) \phi\right]. \tag{2.23}$$

In the former expressions, both the pressure P and surface tension σ act as Lagrange multipliers throughout the simulation. The equation for the spacial and temporal evolution of the order parameter ϕ are now concluded and as such the simulations can proceed, something to be further explained on the computational simulations chapter.

2.3 2D mRNA Transport Model

The second model will focus more on the biological concept of mRNA localization by axonal transport. This approach is slightly different: instead of developing a brand new model, the option was to adapt and implement two different models into a new and unified one. For the axonal growth, the model will be adapted from the angiogenesis model by Travasso *et al.* [40] while the microtubule transport will be inspired in the model by Szymanska *et al.* [31], with a phase field adaptation based on the articles by Kockelkoren *et al.* [41].

The phase field model chosen can be adapted to describe axonal growth. This model is constituted by two PDEs that here will describe the time evolution of the two components of the system: the attractive chemical cue outside the cell, T, and the shape of the neuron, given by an order parameter ϕ evolution in all the space. The model also has two other equations that address the dynamics of the GC: one describes its velocity $\vec{v}_{GC}$ and the other its order parameter ϕ_{GC}.

In this model and analogously to the biological one, the chemical signal evolution heavily depends on both diffusion of the growth factor throughout the environment surrounding the cell and its consumption by the neuron

$$\frac{\partial}{\partial t}T = \nabla \cdot (D_i(\vec{r})\nabla T) - \alpha_T T\phi\Theta(\phi). \tag{2.24}$$

The diffusion coefficient, $D_i(\vec{r})$, depends on the type of chemical cue present in the environment, although in this model it is considered a constant. The second term is the consumption of the signal by the growing cell, with α_T the consumption rate. The Θ represents a Heaviside function (see Appendix section A.4).

The time evolution of the order parameter ϕ is as follows, considering both a dynamic and a proliferative term

$$\frac{\partial}{\partial t}\phi = M\nabla^2\left(-\phi + \phi^3 - \epsilon\nabla^2\phi\right) + \alpha_p(T)\phi\Theta(\phi). \tag{2.25}$$

The dynamics are described by the previously mentioned *Model B* physics. M represents the mobility coefficient for the growth cone and α_p the growth rate.

The GC will advance at a determined velocity, $\vec{v}_{GC}$, that proportionally depends on the growth factor $G = |\nabla T|$

$$\frac{d}{dt}\vec{r} = \vec{v}_{GC} = \chi\nabla T\left[1 + \left(\frac{G_m}{G} - 1\right)\Theta\left(G - G_m\right)\right]. \tag{2.26}$$

with χ the chemotactic response of the membrane of both the GC and the rest of the axon, while G_m is the minimum value to trigger a chemotactic response of the cell.

However, the velocity equation above does not influence either of the other two aforementioned equations, only because it is not a general parameter but rather a GC one. With that said, this particular part of the neuron will have a different order parameter, inversely proportional to the velocity but also dependent on the growth rate of the axon.

$$\phi_{GC} = \frac{\alpha_p(T)\pi R_{GC}}{2|\vec{v}_{GC}|} \tag{2.27}$$

with R_{GC} the radius of the growth cone. In this model, the morphology of this structure is not considered, as the only focus will be on the dynamics and therefore it can be simplified into a circumference.

Finally, in this part of the model, there is also a microtubule formation which is basically the log of positions of the GC, in the middle of the axon, which will be further described in the simulation method.

The second part of the model has to do with the internal dynamics of actin. The equations

for the time evolution of both proteins and mRNA, whether free or bounded to the microtubules, are inspired by the equations developed by Szymanska *et al.* [31]. However, these equations have to be adapted to the PFM. The approach used is very similar to the one developed by Kockelkoren *et al.* [41], which implies the multiplication of the internal equations by the order parameter, localizing the concentrations inside the cell.

Firstly, the mRNA originates in the nucleus and diffuses throughout the cell. Later, when it encounters the microtubules, it binds them and after a while, it is freed to be translated at the necessary location. There is, however, a different decay rate for each type of mRNA: if it is bounded, it will be more protected from decaying and therefore will last longer. When applying the PFM, the free mRNA concentration is obtained by $m_f\Phi$, where m_f is a field that will be calculated. In this equation, $\Phi = \frac{1+\phi}{2}$ is equal to zero outside the cell and equal to 1 inside the cell. Therefore, the concentration of the free mRNA is located only inside. The diffusion equation is written for $m_f\Phi$, as m_f can be different from zero outside the cell, as seen in the Appendix section A.6.1:

$$\frac{\partial}{\partial t}m_f = \frac{k_d}{\Phi}\nabla^2\left(m_f\Phi\right) - \lambda_f m_f - \gamma m_f \xi\left(\frac{M_m - m_l}{M_m}\right) + \frac{\beta_m\left(1-\xi\right)m_l}{\xi\Phi} \tag{2.28}$$

with k_d the diffusion constant, λ_f the free mRNA decay, β_m the probability of unbinding of the mRNA to the microtubule, ξ the microtubule density function, γ a binding constant and M_m the maximum concentration of linked mRNA for each point (i, j). It is easy to see all life stages of the free mRNA: the diffusion term, the decaying term (where λ represents the probability of decay) and the terms related to the dynamics with the microtubules: the binding (proportional to the concentration of free mRNA, the presence of microtubules and the cutoff term representing the maximum concentration of linked mRNA) and finally the unbounding (with a probability β_m of unbinding, depending on the microtubule density).

The microtubules are not present only at the centre of the axon but also can appear closer to the membranes. The microtubule density function is a Gaussian function, centred in the microtubule created with the axonal growth.

The equation for the time evolution of the linked mRNA has symmetrical counterparts to some of the terms (binding/unbinding). However, the mRNA no longer diffuses but rather travels through the microtubules. As the linked mRNA only depends on the presence of microtubules, the equation will be independent of the order parameter Φ:

$$\frac{\partial}{\partial t}m_l = -\nabla\cdot\left(v_m\left(\frac{M_m - m_l}{M_m}\right)m_l\mathbf{v}\right) - \lambda_f m_l + \gamma m_f\Phi\xi\left(\frac{M_m - m_l}{M_m}\right) - \frac{\beta_m\left(1-\xi\right)m_l}{\xi} \tag{2.29}$$

where v_m is the absolute value of the velocity of the linked mRNA, $\mathbf{v}$ the vector field of the microtubules and λ_l the linked mRNA decay. This final model is the adaptation of the aforementioned methods, which allows both an axon growth and guidance while complementing it with the local mRNA translation occurring along the axon and mainly in the GC.

Chapter 3

Computational Simulations

Although the presented models are described by different conditions and equations, they were both developed using the C programming language. In addition, the integration of the PDEs was done using a time-step dependent algorithm, namely the explicit Euler Method (see Appendix section A.7). The flow chart for the integration is represented in the Figure 3.1.

The programs were divided between several functions. For example, each mathematical operator (e.g. Laplacian, divergence - see Appendix section A.8) had its own function, as well as the initialization of variables and systems or any sort of matrix calculations. There were, however, some functions common to both the simulations.

As the implementation was done in C,each matrix was represented by a double or triple pointer of base type *double*, which represented either a 2D or a 3D system. A pointer is a variable that indicates the direct address of the memory location of another variable. In the case of a 2D matrix, it works as a pointer that indicates the address of a list of pointers (a "vector"), and each of the pointers in that list indicates a list of values. At the end of the program, however, there is also the implementation of a function which aims to free the memory allocated for each matrix, therefore allowing other processes to use it.

Some other matrix-related functions are important, namely one to assign a value to all the points in the matrix or printing the said matrix into a file, so it can be later analysed. There are, also, small functions to implement simple matrix relations, such as multiplication, addition, or even a dot product between two small vectors.

Lastly, it is relevant to refer that the boundary conditions for both models are periodical, meaning an object disappearing in one boundary will appear with the same dynamical conditions in the other.

In this chapter, as the evolution of the models was progressive, both the simulation and their results will be presented, along with the discussion for each topic.

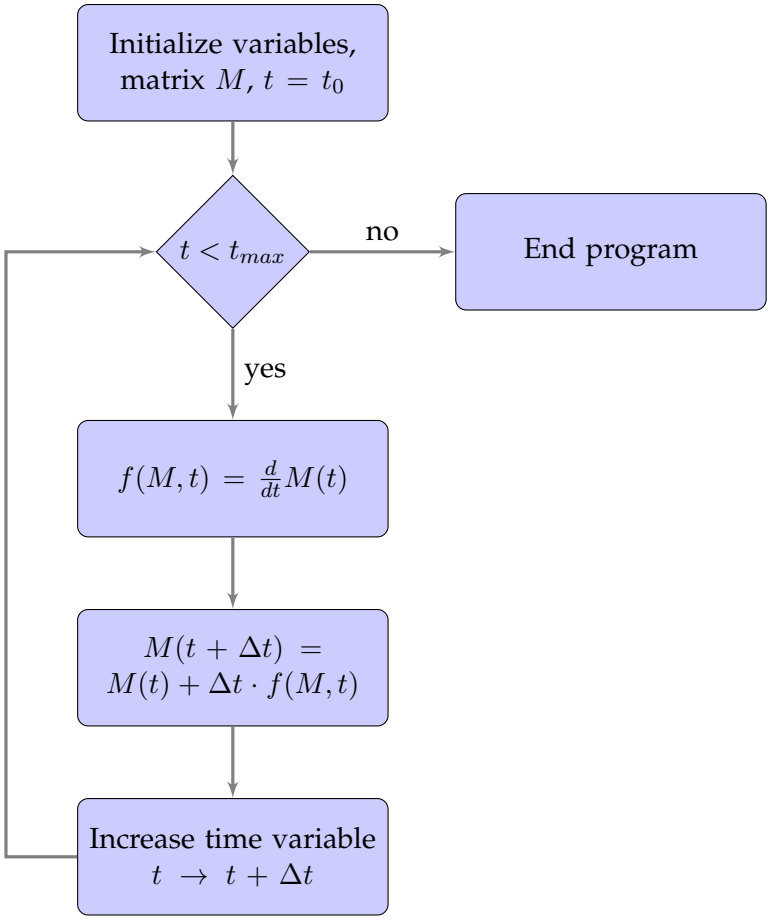

FIGURE 3.1: Flowchart of a basic Euler method algorithm, considering matrix M, time variable t, time step Δt and function $f(M,t)$ computed for each point in the (discrete) space.

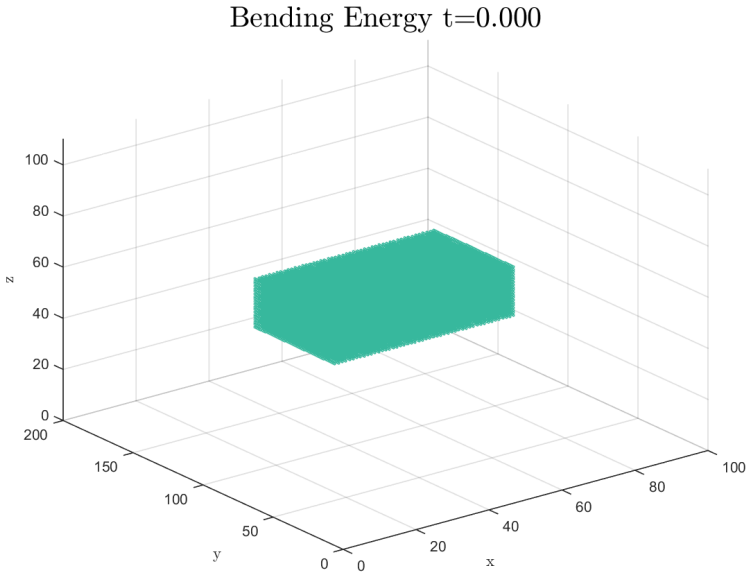

FIGURE 3.2: Initial Condition for the 3D Shape and Forces Model. The parallelepiped in the centre of the figure represents the region for $\phi = 1$.

3.1 3D Shape and Forces Model

The principal idea for this model is to consider the cell as a region in the three dimensional space. To have a successful model, each of the different components of the mathematical method has to be progressively tested to guarantee the stability of the simulation. As the total energy equals the sum of the different energies, it was necessary to confirm that each stage was done properly before advancing. In the next subsections, each of the steps will be further explained and analysed. The initial conditions for the simulations are presented in Table 3.1.

As shown in Figure 3.1, the first step is to initialize the variables which in this case will be defining the order parameter for the entire system, which will be $\phi = 1$ inside the cell and $\phi = -1$ outside. The length of each cell side was calculated pondering both area and volume considerations, so as to force the spherical proportionality $V = \frac{1}{6}\left(\frac{A^3}{\pi}\right)^{\frac{1}{2}}$ between the two (see Appendix section A.5.4). As the first input is the initial intended surface area, the rest is calculated afterwards.

As it was previously stated, the computational program is implemented according to the Euler algorithm. The equations explained in the previous chapter are applied as demonstrated in the flowchart in Figure 3.3, although each part is further explored below.

TABLE 3.1: Initial Conditions for the 3D Model Simulations. These are the optimal initial conditions for the model, even though there are constants not used in the all the simulations: k_2 and α_V are not used in the first simulation, α_A is only used in the last two simulations. * - Although this value is represented as an initial condition, it is only activated later in the simulation (explained in the subsection 3.1.3) and not when $t = 0$.

Δt	0.005
Δx	1
Box Size	100x200x120
Initial Area	10000
Maximum Volume	≈ 94032
Initial Volume	≈ 56419
X Side Length	50
Y Side Length	≈ 57.97
Z Side Length	≈ 19.47
ϵ	1
k_1	1
k_2	2
α_V	0.0005
α_A	0.0005*

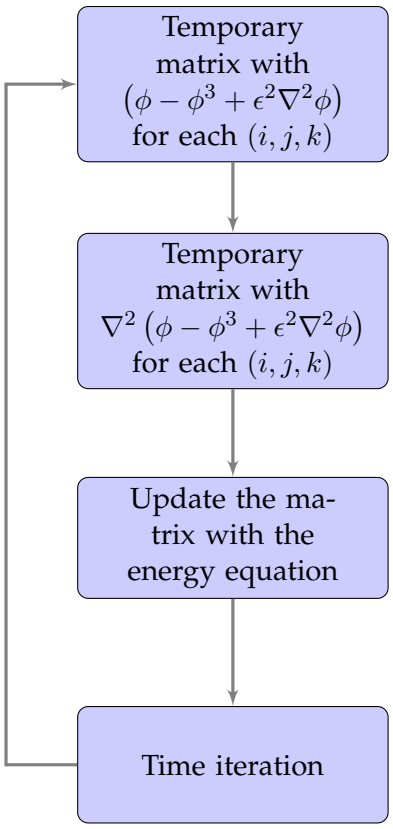

FIGURE 3.3: Flowchart for the matrices involved in the iterations for the 3D Shape model.

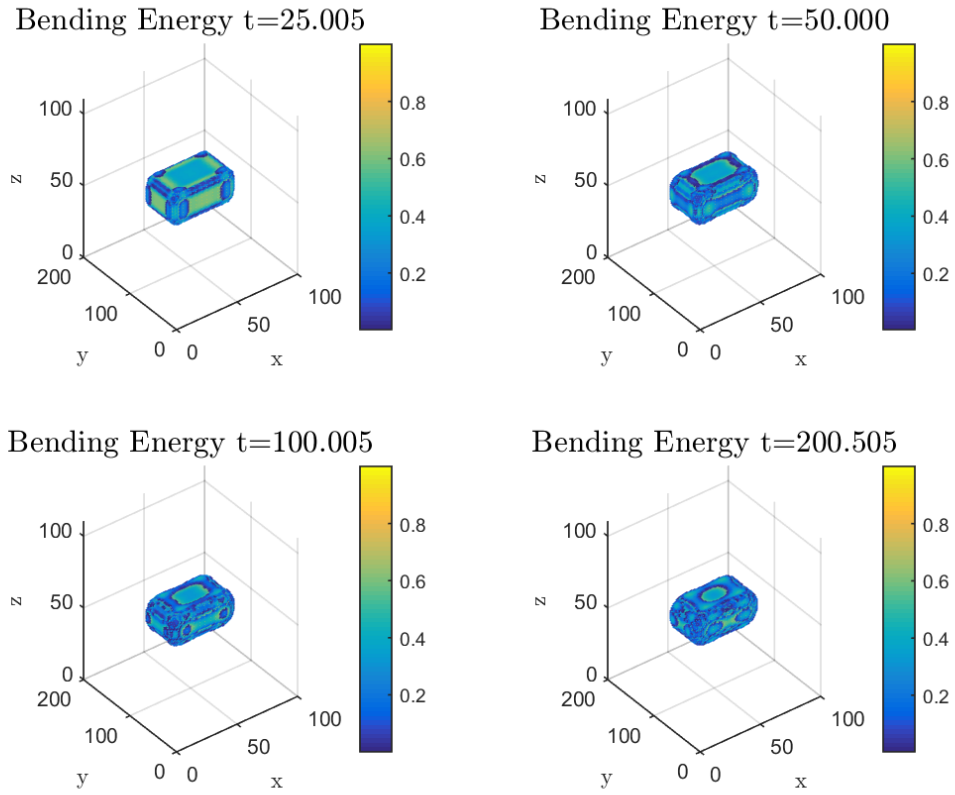

FIGURE 3.4: Time evolution of the 3D Shape, with only the bending energy activated. The colorbar represents the positive range of the order parameter, i.e., the interior of the cell.

3.1.1 Simulation 1 - Bending Energy

The first part of the simulation is about having a stable 3D shape so as to guarantee that all the further steps occur correctly. In this step, the order parameter equation is only represented by $\frac{\partial \phi}{\partial t} = -\frac{\delta E_b}{\delta \phi}$ (Equation 2.18) . In Figure 3.4, the time evolution of the shape for $t = 25.005$, $t = 50.000$, $t = 100.005$ and $t = 200.505$ is represented. As it is clearly visible in the graphics from Figure 3.5, the time evolution of both area and volume is not stable, which is why the next steps are important.

The initially parallelepiped shape will tend to round its corners, as the stabilizing shape with the minimum bending energy is a sphere. This tendency will be constant throughout the rest of the simulations.

3.1.2 Simulation 2 - Volume Conservation

As of now, the equation representing the order parameter has another term for the energy: the volume stabilization using the bulk pressure P. However, this is not a constant but rather a variable whose value is updated with each iteration. It consists in a constant α_v times the difference between the ideal (initial) volume V_i and the actual volume from the previous iteration.

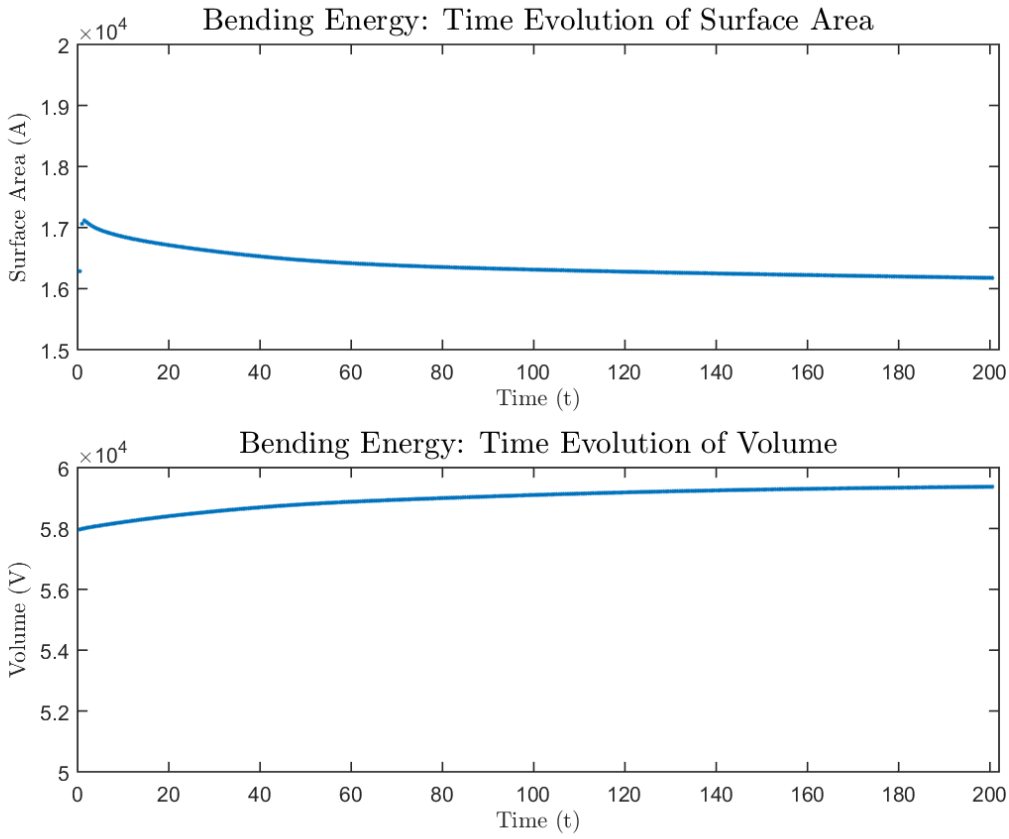

FIGURE 3.5: Time evolution of the surface area and volume of the 3D shape, with only the bending energy activated. Both appear to have monotone behaviours: the surface area is decreasing and the volume increasing.

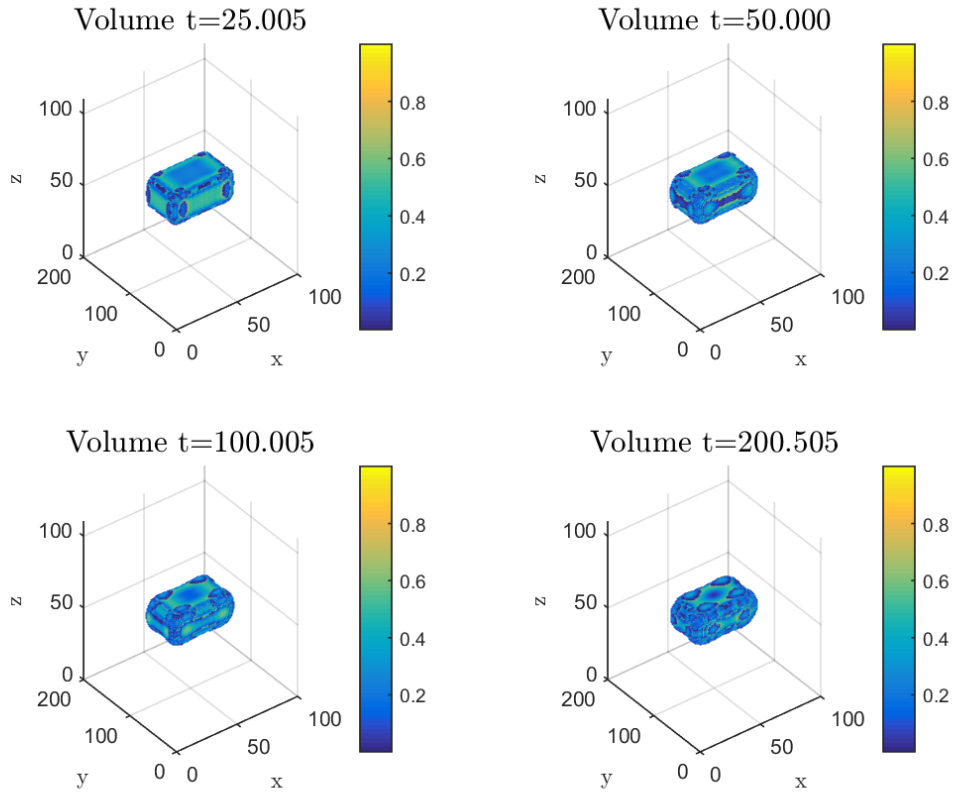

FIGURE 3.6: Time evolution of the 3D Shape, with the bending energy and volume conservation activated. The colorbar represents the positive range of the order parameter, i.e., the interior of the cell.

$$P(t + \Delta t) = P(t) + \alpha_V (V_i - V_{old}). \tag{3.1}$$

The volume is calculated each iteration as

$$V_{old} = \sum_{i,j,k} \left(\frac{1+\phi}{2} \right)^2 (2 - \phi)\,. \tag{3.2}$$

In other words, for each t, the program starts with a variable $V_{old} = 0$ and, for each point (i, j, k), adds the above term and then calculates the new pressure. The results of the simulation with the two first energy terms ($\frac{\delta E_b}{\delta \phi}$ from Equation (2.18) and $\frac{\delta E_v}{\delta \phi}$ from Equation (2.21)) are presented in Figure 3.6, for $t = 25.005$, $t = 50.000$, $t = 100.005$ and $t = 200.505$.

Although the shape is very similar to the previous simulation, the volume is stable throughout the time evolution, as seen in Figure 3.7. However, it is still quite visible that the surface area is not stabilized.

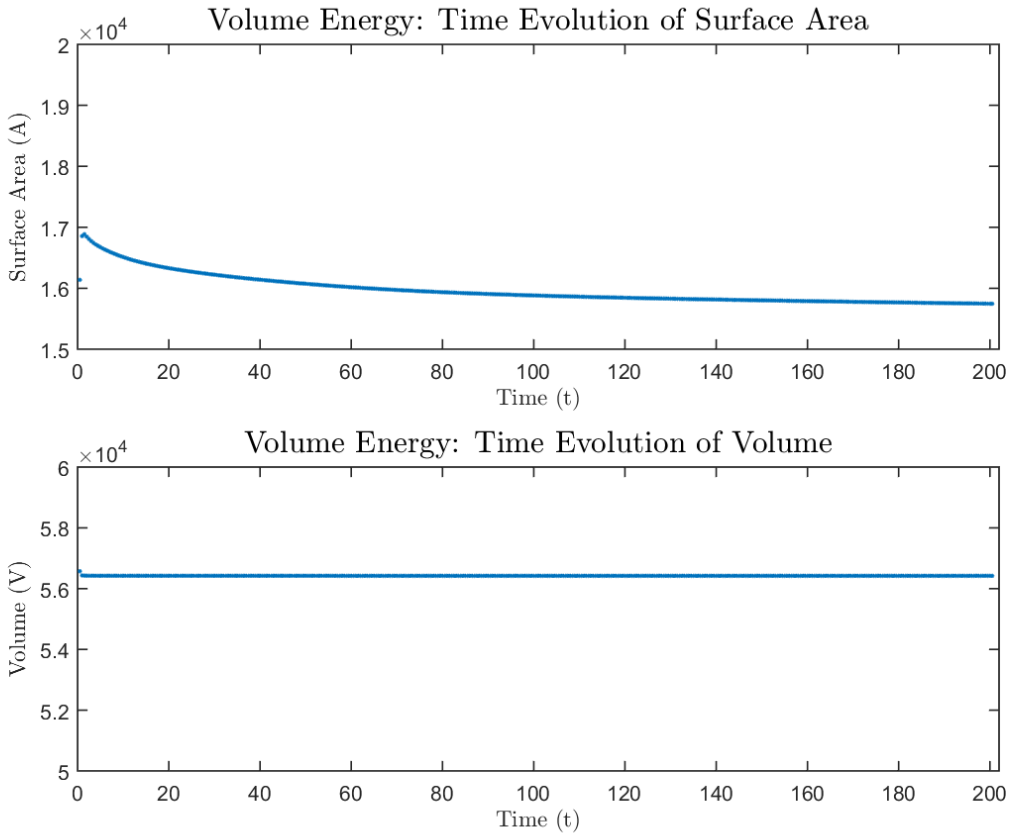

FIGURE 3.7: Time evolution of the surface area and volume of the 3D shape, with the bending energy and volume conservation activated. While the surface area is decreasing, the volume is stabilized.

3.1.3 Simulation 3 - Surface Area Stabilization

The last step before applying forces to the system is the total surface area conservation throughout time. As stated before, it depends on the surface tension σ which, in turn, represents a proportionality to the difference between the intended surface area and the one calculated in the latest iteration

$$\sigma(t + \Delta t) = \sigma(t) + \alpha_A \left(A_i - A_{old}\right). \tag{3.3}$$

However, this term is only activated after a certain time as passed ($\approx t = 3.55$, value obtained from several runs of Simulation 1) to make sure the volume is already stabilized. The surface area is calculated as

$$A_{old} = k_2 \sum_{i,j,k} \left(1 - \phi^2\right)^2. \tag{3.4}$$

Similarly to the volume, the sum represents the addition of the above term in each point (i, j, k). In Figure 3.8 is represented the simulation with the three energy terms, for $t = 25.005$, $t = 50.000$, $t = 100.005$ and $t = 200.505$, with the consequent surface area and volume graphics in Figure 3.9.

The shape of the cell is much less deformed with both terms activated, as it is visible comparing the Simulation 3 Figure 3.8 with Simulation 1 Figure 3.4 and Simulation 2 Figure 3.6. As the shape stabilization was achieved, the mechanical forces can now be applied so as to try to create the protrusion.

3.1.4 Simulation 4 - Mechanical Forces

To implement the final term of the equation, the mechanical forces were constricted to a region in the space, with interface present, and where there are force vectors. The interaction of the force vectors with the membrane acts like represented in equation (2.19): the scalar product between the force density vector $\vec{F}$ and the vector $\vec{r}$ for each point (i, j, k). As a side note, it is easy to observe that the order parameter dependence is the same as the one for the surface area (see Equations (2.19) and (2.23)). The results for the simulation, with $t = 11.000$, $t = 12.000$, $t = 13.000$ and $t = 14.000$, are present in Figure 3.10.

The results are not at all the expected. The time frame shown is much smaller than the previous simulations because the next iteration resulted in a complete interface destruction. In other words, although the first three terms of the equation alone produce a stable result, when the forces are added, the interaction does not work properly. The hyperbolic tangent profile does not survive the introduction of this energy term. Due to time constraints, this simulation could not be further explored. It also had the characteristic of being extraordinarily slow. In all the simulations ran, the steady state was not achieved even after several days running. With this in mind, a new model was developed and simulated, originating different type of results with a different approach.

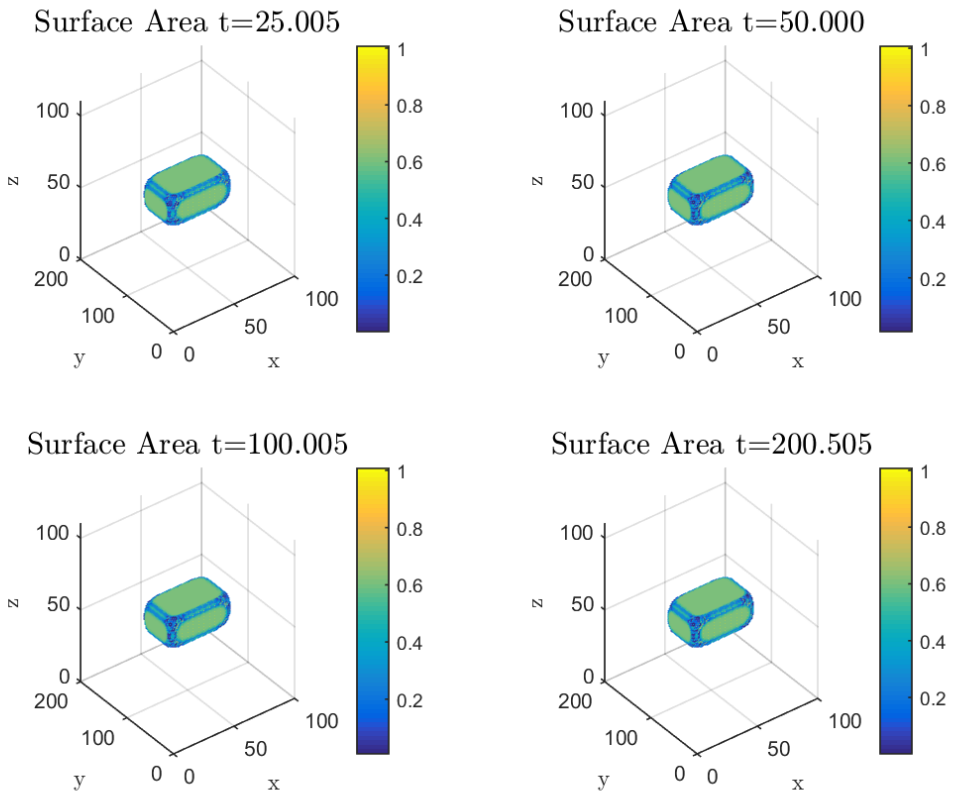

FIGURE 3.8: Time evolution of the 3D Shape, with the bending energy, volume conservation and surface area stabilization activated. The colorbar represents the positive range of the order parameter, i.e., the interior of the cell.

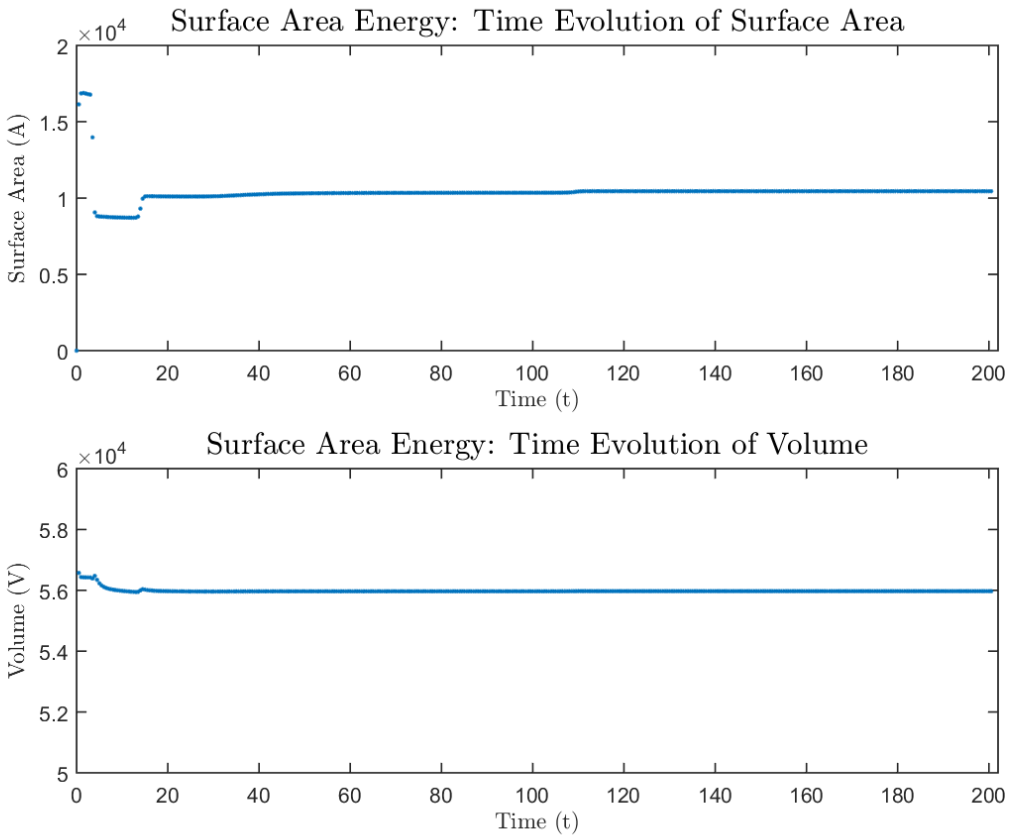

FIGURE 3.9: Time evolution of the surface area and volume of the 3D shape, with the bending energy, volume conservation and surface area stabilization activated. The conservation of both volume and surface area is indeed achieved after a while, since the activation of the surface area term in the equation happens after the initial stabilization of volume.

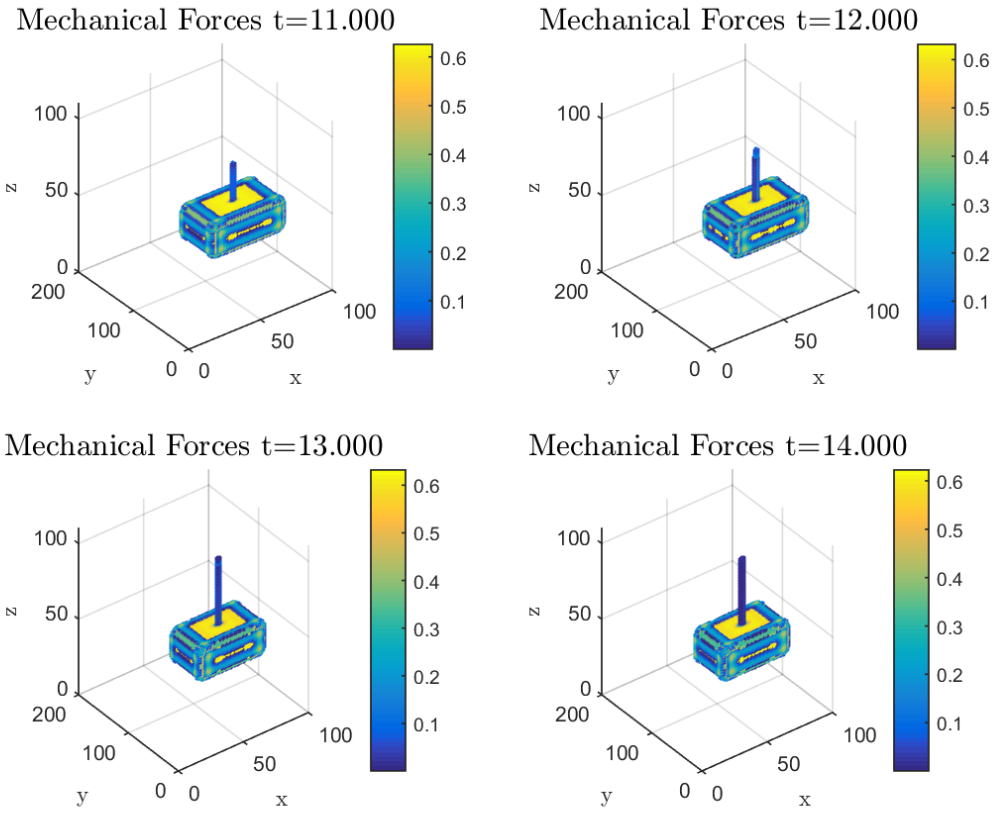

FIGURE 3.10: Time evolution of the 3D Shape, with all the components of the equations activated. The colorbar represents the positive range of the order parameter, i.e., the interior of the cell.

3.2 2D mRNA Transport Model

Although the first model presented in this work was made entirely from the beginning by the author, this second one will be implemented differently. As the first part of the model was an adaptation from the work by Travasso *et al.* [40], the computational counterpart was also an adaptation from their work, functioning almost as a black box for this model (Figure 3.11).

Initially, the neuron starts as a circumference with $\phi = 1$ and the rest of the system as $\phi = -1$ (see Figure 3.12). Around the matrix there are growth factors that induce the formation of the GC. As soon as it is formed, it starts moving away from the cell body and thus creating the beginning of the axon.

Each centred position of the GC will be registered as the coordinates for the microtubules, present in the middle of the axon. After a few iterations, the mRNA transport program will be activated.

First of all, the value interval of the order parameter is changed to $\phi \rightarrow \Phi \in [0, 1]$ for simplification in the implementation of the equations. The next step is the formation of the microtubule vectors and density function. Each MT is initially represented as a vector calculated with the coordinates from the point lying five positions ahead, i.e., that links positions by which the GC has passed through, separated by five units. Afterwards, a diffusion process is applied to guarantee both continuity of the vector field as well as for it to be more biologically relevant: the MT are displayed throughout the axon, with a larger concentration in the middle. The MT density function, ξ, is obtained from this diffusion process.

The initial conditions for the mRNA concentration matrices depend on whether it is the first run of the program or not. Basically, if there are already existing matrices from previous runs then they will be the initial conditions for the present run. Otherwise, the matrices start with $m_f = 1$ in a centred circumference, the nucleus, and $m_f = 0$ everywhere else, while the concentration for linked mRNA will be zero in the entire system. The values for the other variables are presented in Table 3.2.

As mentioned before, there is a part of the cell body that is analogous to the nucleus. With a radius of 10 points, it is the only part of the cell where there is no mRNA decay, meaning it only diffuses from there and the value is always a constant in said region. The linked concentration only depends on the presence of microtubules and, as such, it is always zero inside the cell body.

The equations are only calculated for each point (i, j) where the value of ϕ is above the threshold (shown in Table 3.2), so as to avoid numerical problems arising from divisions by numbers close to zero. The components of the equations that are divided by the MT density function also follow the same rule, since $\xi > 0$ only at the axon.

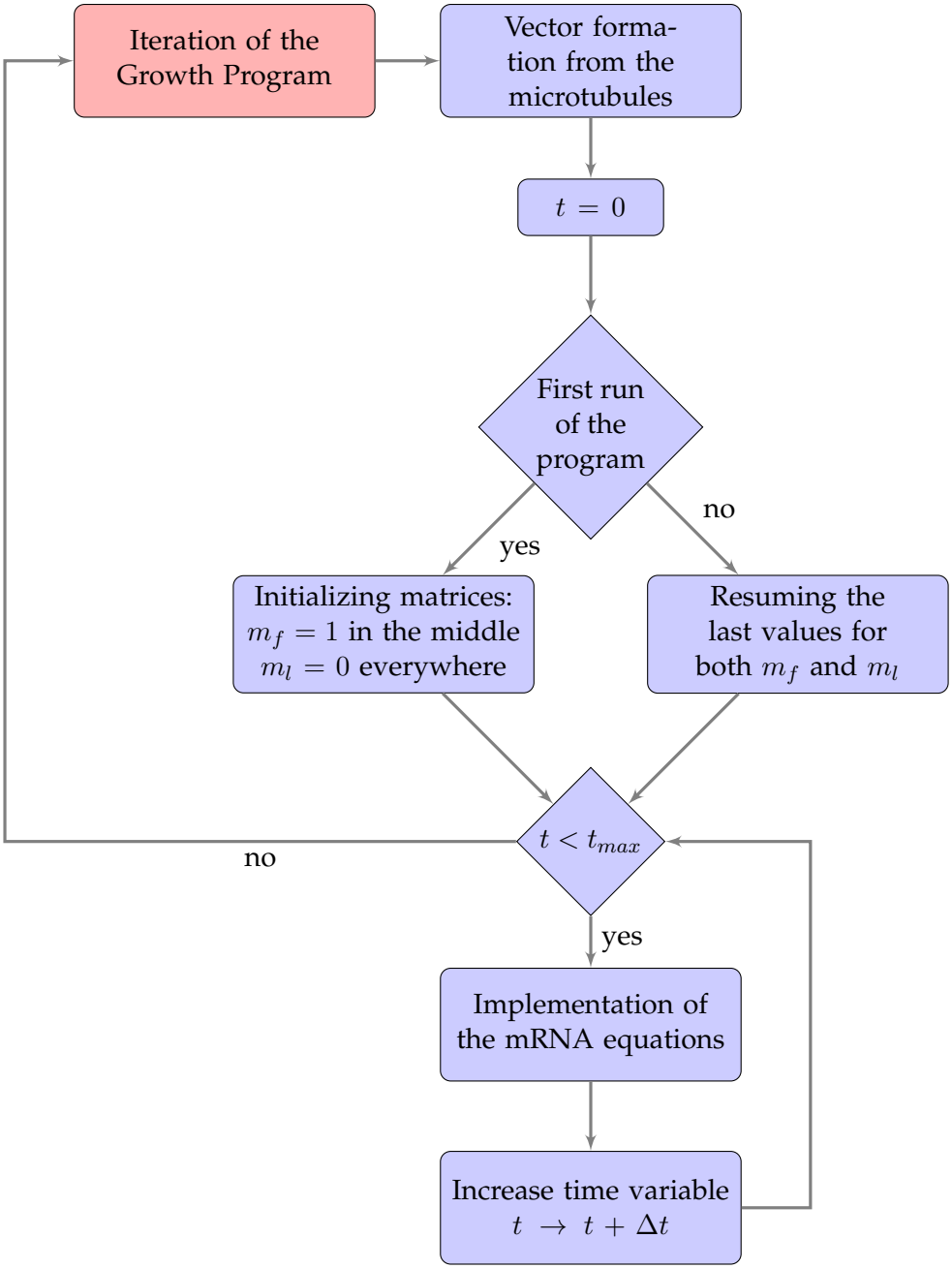

FIGURE 3.11: Flowchart for the 2D mRNA Transport Model. The red block represents the program for the axonal growth, while the blue blocks represent the steps in the modelling of the mRNA transport.

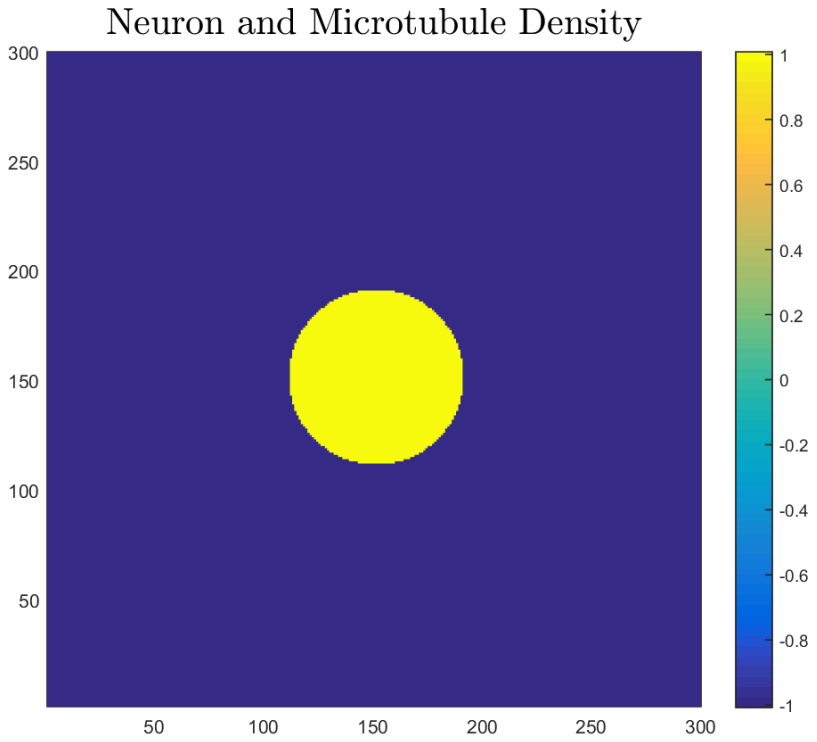

FIGURE 3.12: Initial Condition for the 2D Model. The colorbar represents the order parameter. Although in this part the interval is $[-1, 1]$, further ahead it will be shifted to the interval $[0, 1]$

TABLE 3.2: Constants for the 2D Model Simulations. These are the optimal values for the model, obtained from both literature [31] and by trial-error with the simulations.

Box Size	300x300
Δt	0.005
Δx	1
k_d	10
λ_f	0.005
γ	1
M	1
β_m	0.01
v_m	1
λ_l	0.001
Nucleus radius	10
Threshold	10^{-8}

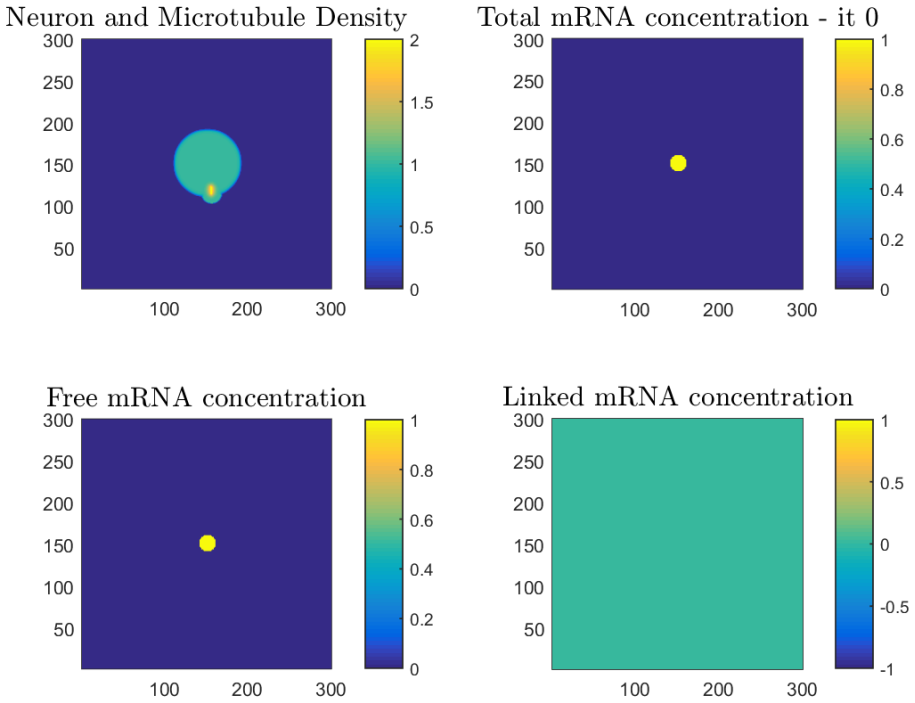

FIGURE 3.13: First iteration of the 2D Model. Top left: Neuron and Microtubule Density, the neuron matrix is between the interval $[0, 1]$. Top right: Total mRNA concentration (linked + free) in the cell. Bottom left: Free mRNA concentration, only in the "nucleus". Bottom right: Linked mRNA concentration, which is zero in the entire system.

Afterwards, the Euler algorithm is applied. Some temporary matrices are calculated, such as the Laplacian for the free mRNA concentration or the divergence for the linked mRNA. When the transport program reaches the maximum time, it allows the growth to continue by running some iterations of the axonal growth code. The cycle ends when the growth maximum time is reached.

In Figure 3.13, it is possible to see the initial conditions for a first run of the mRNA transport model, which happened at the iteration number 23000 of the axonal growth program.

After a few iterations, the free mRNA diffuses from the centre and reaches the tip of the MT density. In that case, as shown in Figure 3.14, the linked mRNA concentration is no longer zero, although still very small. From now on, the free mRNA also appears in the axon, outside the cell body: the unbinding term of the linked mRNA equation is activated. It is possible to see, when t reaches t_{max} that the linked mRNA has reached the final end of the MT (Figure 3.15). At that point, the program ends and the growth continues for more iterations, before the transport is activated again.

When the transport program is re-initiated, it recovers the last position of the concentration, calculates the new vectors and continues the transport as if there was no stop. In

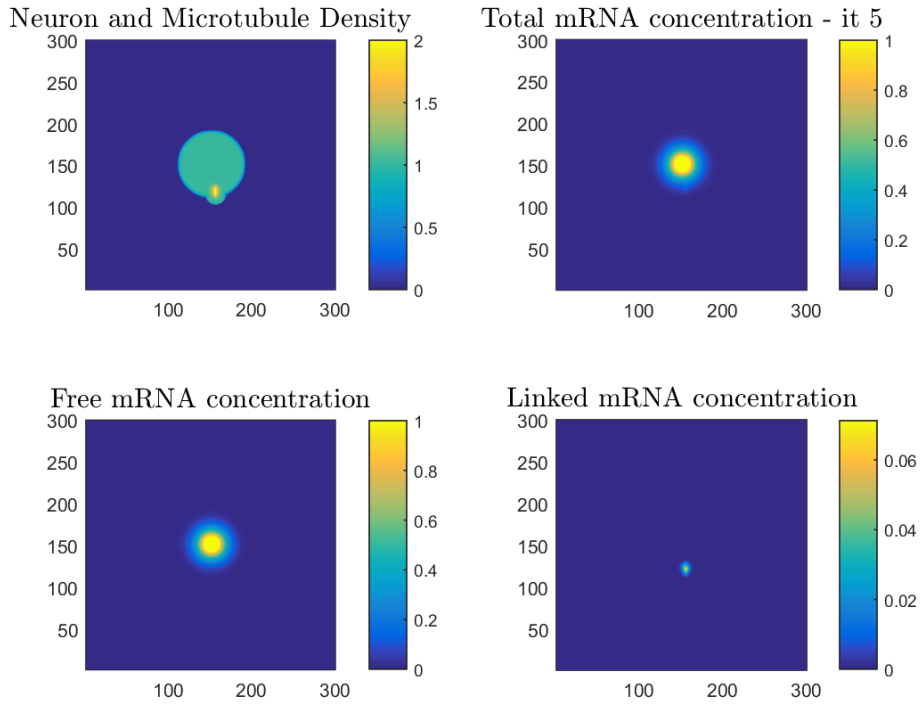

FIGURE 3.14: After a few iterations of the 2D Model, there are some notable changes. Top left: Neuron and Microtubule Density, the neuron matrix is between the interval $[0, 1]$. Top right: Total mRNA concentration (linked + free) in the cell. Bottom left: Free mRNA concentration, now not only in the cell body but also has been unbounded from the MT in the axon. Bottom right: Linked mRNA concentration, only present in the MT density function area.

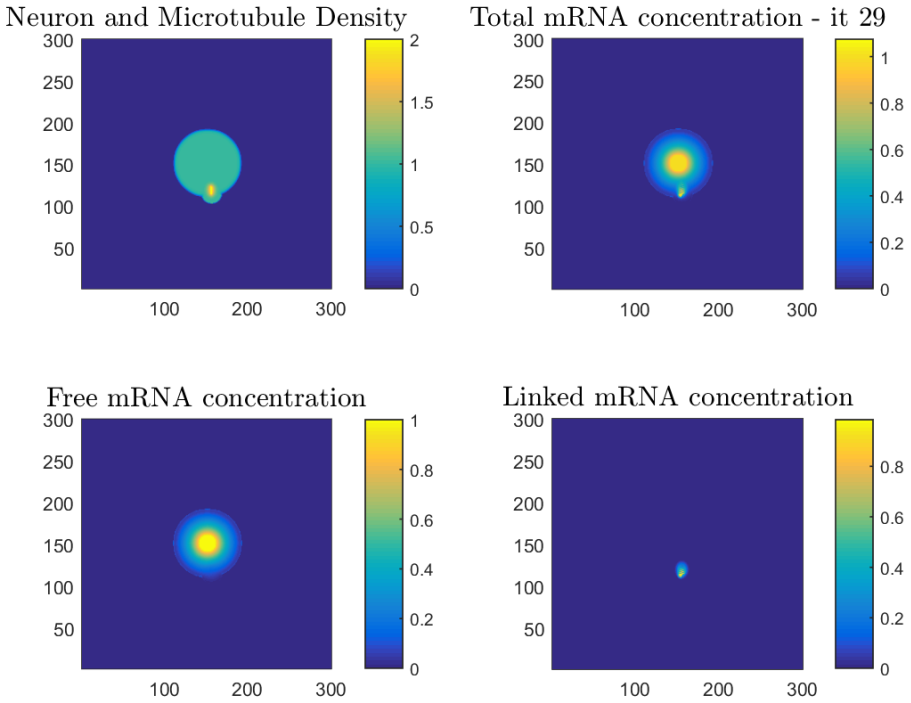

FIGURE 3.15: Last iteration of the first run of the mRNA transport program. Top left: Neuron and Microtubule Density, the neuron matrix is between the interval $[0, 1]$. Top right: Total mRNA concentration (linked + free) in the cell. Bottom left: Free mRNA concentration. Bottom right: Linked mRNA concentration.

Figures 3.16 and 3.17, it is represented the third run of the program (first and last iteration, respectively, with the last concentration values of the second run as the starting point). After a while, it again reaches the end of the MT and by the end of both programs, the axon has grown along with the regular and consistent transport of the mRNA, as envisioned at the start (Figure 3.18).

The results of this model agreed with what was expected: with a stabilized cell, a vector field for the MT and a consequent MT density function, the equations worked properly and the mRNA transport was successful from the nucleus to the GC, a great foundation for more complex models.

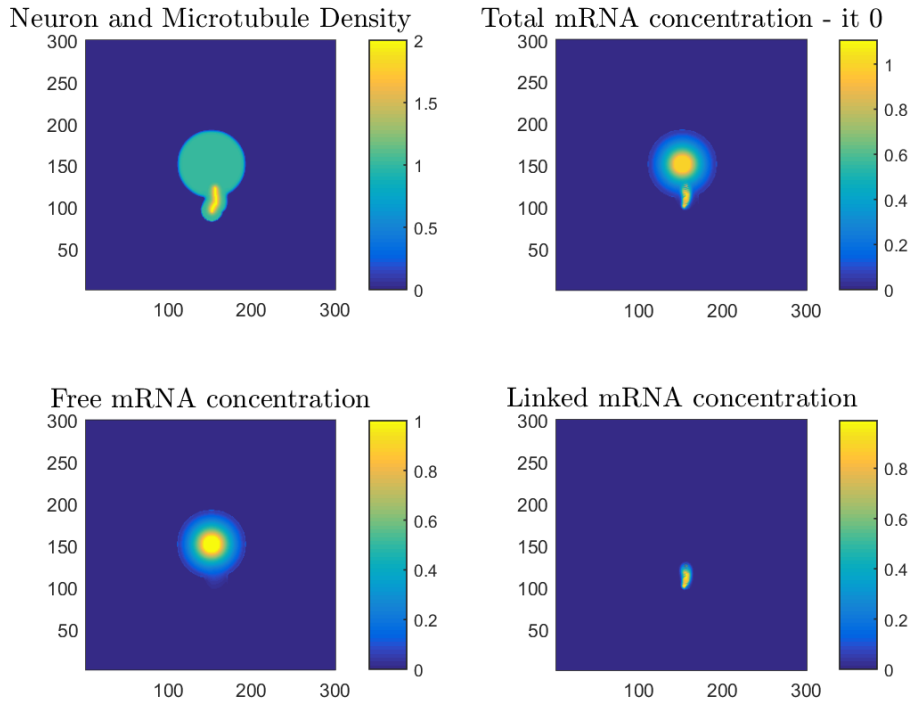

FIGURE 3.16: First iteration of the third run of the mRNA transport program. Top left: Neuron and Microtubule Density, the neuron matrix is between the interval $[0, 1]$. Top right: Total mRNA concentration (linked + free) in the cell. Bottom left: Free mRNA concentration. Bottom right: Linked mRNA concentration.

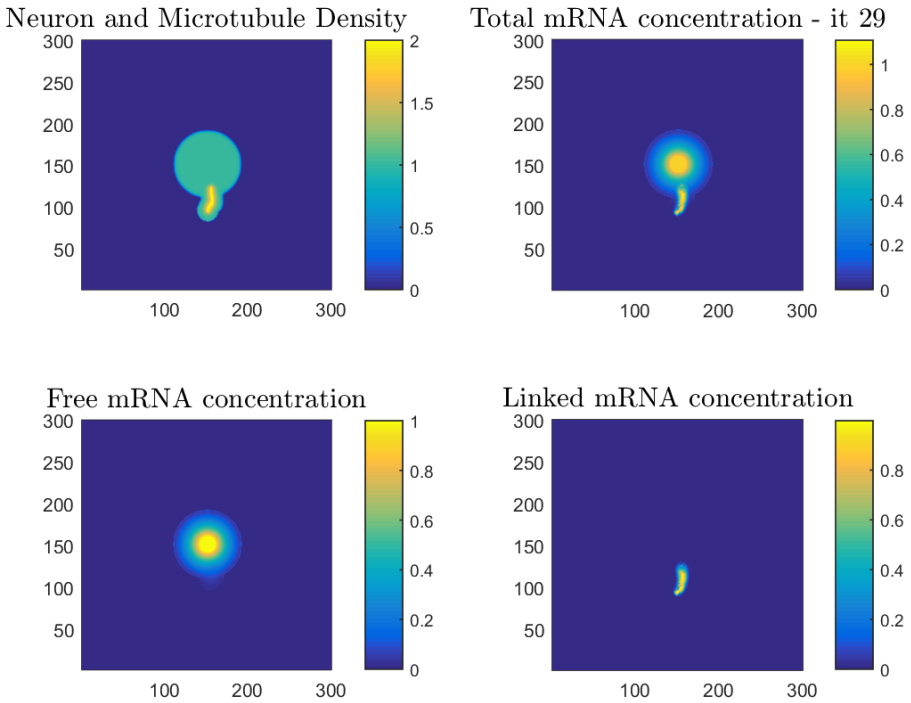

FIGURE 3.17: Last iteration of the third run of the mRNA transport program. Top left: Neuron and Microtubule Density, the neuron matrix is between the interval $[0, 1]$. Top right: Total mRNA concentration (linked + free) in the cell. Bottom left: Free mRNA concentration. Bottom right: Linked mRNA concentration.

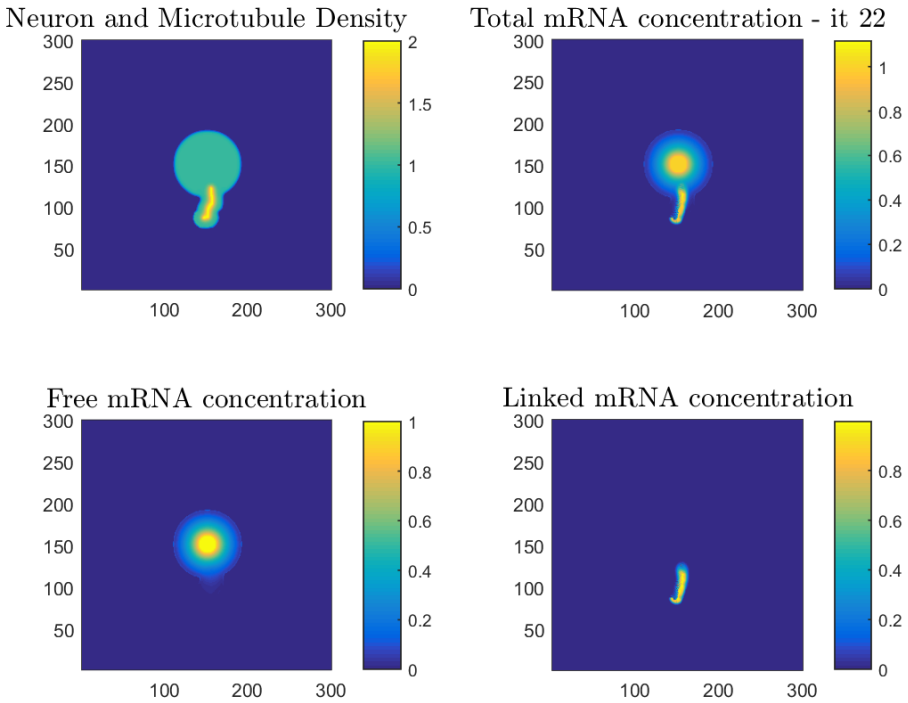

FIGURE 3.18: Last iteration of the last run of the mRNA transport program. Top left: Neuron and Microtubule Density, the neuron matrix is between the interval $[0, 1]$. Top right: Total mRNA concentration (linked + free) in the cell. Bottom left: Free mRNA concentration. Bottom right: Linked mRNA concentration.

Chapter 4

Conclusions and Future Work

The local mRNA transport in neurons and particularly in axonal growth is a very recent discovery in the field. As such, the data that can be obtained from experimental work is still far from providing all the needed information and therefore can not be properly used to tune mathematical models quantitatively, only with qualitative approximations. In the foreseeable future, there will be many possibilities to perfect the simulations here presented, resulting in the natural improvement of these mathematical models.

The 3D shape model was ambitious from the start: not only was it a novel idea as it was also implemented in three dimensions. In other words, a new model, without guarantee of successful results, implemented for a number of dimensions that increases significantly the time required for each simulation in comparison to other models of the same structure.

The time frame constraint was inevitable. Each simulation, with thousands of iterations and up to the fourth derivative each, was a slow process and the program debugging was done in a span of several days as each run took close to a day. And although the first three parts of the modelling were successful and a stable cell shape achieved, which by itself is a great foundation for further work, the fourth was an unsuccessful successor. The interaction between the mechanical forces and the interface caused the destruction of the latter and consequently of the entire system.

Without the time setback, the model can be further developed if the mechanical forces are more thoroughly looked into and if the simulations can occur for an unbounded amount of time. The main question remaining is how does the interaction with the forces destroy the otherwise stable interface, with perhaps some focus on the implementation of said forces in the computational model.

The approach for the 2D mRNA Transport model was completely different. The main focus was a proof of concept: the inner works of the cell could and do influence the outcome of the morphological growth, which was clearly seen by joining two different type of models into one. While this was successfully reached in this model, there are many ways to further explore and pursue this concept.

The morphological counterpart, that in this case was adapted from a model of a completely different type of biological system, could possibly be adapted from already existing

and successful neuronal growth models, such as the one by Najem and Grant [33].

Regarding the pure aspects of this model, some features could be added to improve the biological veracity: the mRNA binding, unbinding and even production depends on the external stimuli (in this particular case, the attractive growth factors) and the movement of the GC depends on the concentration of both mRNA and proteins, which have to be incorporated into the model, either by transport from the cell body to the GC or by production via mRNA (translation of the localized mRNA).

Concluding, while the first model was unsuccessful at the end, the second proved to be a starting ground to model a recently discovered and particularly difficult biological process, which can be further explored in future investigations.

Appendix A

Mathematical Formulas and Deductions

A.1 Vector Calculus

Vector $\vec{A}$ with coordinates (x, y, z). s a common variable. Function f.

$$\nabla = \left(\frac{\partial}{\partial x}, \frac{\partial}{\partial y}, \frac{\partial}{\partial z}\right) = \frac{\partial}{\partial x}\hat{i} + \frac{\partial}{\partial y}\hat{j} + \frac{\partial}{\partial z}\hat{k} \tag{A.1}$$

$$\frac{d}{ds}\left(f\vec{A}\right) = \frac{df}{ds}\vec{A} + f\frac{d\vec{A}}{ds} \tag{A.2}$$

$$\nabla \cdot \left(f\vec{A}\right) = \nabla f \cdot \vec{A} + f\nabla \cdot \vec{A} \tag{A.3}$$

A.2 Useful Mathematical Equalities

Functions f,g.

$$(a+b)^3 = a^3 + 3a^2b + 3ab^2 + b^3 \tag{A.4}$$

$$\int fgdx = \left(\int fdx\right) \cdot g - \int \left(\int fdx'\right) g'dx \tag{A.5}$$

$$\sinh ax = \frac{e^{ax} - e^{-ax}}{2} \tag{A.6}$$

$$\cosh ax = \frac{e^{ax} + e^{-ax}}{2} \tag{A.7}$$

$$\frac{d}{dx}\sinh ax = a\cosh ax \tag{A.8}$$

$$\frac{d}{dx}\cosh ax = a\sinh ax \tag{A.9}$$

$$\tanh(ax) = \frac{\sinh ax}{\cosh ax} \tag{A.10}$$

$$\frac{d}{dx}\tanh(ax) = \frac{a\cosh(ax)^2 - a\sinh(ax)^2}{\cosh(ax)^2} = a - a\tanh(ax)^2 \tag{A.11}$$

$$\frac{d^2}{dx^2}\tanh(ax) = \frac{d}{dx}\left(a - a\tanh(ax)^2\right) = 2a^2\left(-\tanh(ax) + \tanh(ax)^3\right) \tag{A.12}$$

A.3 Functional Calculus

A *functional* F is a function whose argument is an entire function instead of a single number. Given a quantity f that depends on the space function $\phi(x)$, the functional $F[\phi(x)]$ can be, for example, $F[\phi(x)] = \int f(\phi(x))dx$ [36].

The minimization of a functional $F[\phi(x)]$ in relation to $\phi(x)$ is obtained via *variational derivatives*, by

$$\frac{\delta F[\phi(x)]}{\delta\phi} = 0. \tag{A.13}$$

And, finally, the definition of variational calculus theory:

$$\delta F[\phi(x)] = F[\phi + \delta\phi] - F[\phi] = \int_V \left(\frac{\delta F}{\delta\phi}\delta\phi + \dots\right) dV. \tag{A.14}$$

As for a practical example, given $F[\phi] = \int(\nabla\phi)^2 dx$ and the approximation $\delta F = \int \frac{\delta F}{\delta\phi}\delta\phi dV$,

$$\begin{aligned} F[\phi + \delta\phi] = \int (\nabla(\phi + \delta\phi))^2 \, dV = \int (\nabla\phi)^2 dV + \int 2\nabla\phi\nabla\delta\phi dV \Leftrightarrow \\ \Leftrightarrow F[\phi] + \delta F = \int (\nabla\phi)^2 dV + \int 2\nabla\phi\nabla\delta\phi dV \Leftrightarrow \\ \Leftrightarrow \delta F = \int 2\nabla\phi\nabla\delta\phi dV. \end{aligned} \tag{A.15}$$

Integrating by parts (see Equation A.5), and as the frontier conditions are periodical:

$$\delta F = \int 2\nabla^2\phi\delta\phi dV \implies \frac{\delta F}{\delta\phi} = 2\nabla^2\phi. \tag{A.16}$$

A.4 Dirac's delta function and Heaviside function

The Dirac's delta function or δ function is a linear function, that is defined by

$$\delta(x) = \begin{cases} 0 & x \neq 0 \\ \infty & x = 0 \end{cases} \tag{A.17}$$

and

$$\int_{-\infty}^{\infty} \delta(x)dx = 1. \tag{A.18}$$

The most important property of this function, in relation to the work presented in this thesis, is the following

$$\int f(x)\delta(x - x_0)dx = f(x_0), \tag{A.19}$$

or the analogous for more dimensions

$$\int f(\vec{r})\delta(\vec{r}-\vec{r}_s)dV = f(\vec{r}_s) \tag{A.20}$$

which allows the calculation of the value of any function f at the determined point x_0 or distance $\vec{r}_s$.

Another important characteristic of the delta function is that it represents the derivative of the Heaviside function, Θ.

$$\frac{d}{dx}\Theta(x) = \delta(x). \tag{A.21}$$

This function, also known as the step function, is defined by the following conditions:

$$\Theta(x-x_0) = \begin{cases} 1 & x \geq x_0 \\ 0 & x < x_0 \end{cases}. \tag{A.22}$$

In other words, the function takes the value 0 when the argument is negative and 1 otherwise.

A.5 3D Shape and Forces Model

A.5.1 Deriving ϕ with respect to the space variables

$$\begin{gathered} \partial_i\phi = \partial_i\left(\tanh\left(\frac{1}{\sqrt{2}\epsilon}d(\vec{r})\right)\right) = \left(1-\tanh^2\left(\frac{1}{\sqrt{2}\epsilon}d(\vec{r})\right)\right)\frac{1}{\sqrt{2}\epsilon}\partial_i d(\vec{r}) \Leftrightarrow \\ \Leftrightarrow \partial_i\phi = \frac{1}{\sqrt{2}\epsilon}(1-\phi^2)\partial_i d(\vec{r}) \end{gathered} \tag{A.23}$$

$$\begin{gathered} \partial_j\partial_i\phi = \partial_j\left(\frac{1}{\sqrt{2}\epsilon}\left(1-\tanh^2\left(\frac{1}{\sqrt{2}\epsilon}d(\vec{r})\right)\right)\partial_i d(\vec{r})\right) = \\ = \frac{1}{\sqrt{2}\epsilon}\left(1-\tanh^2\left(\frac{1}{\sqrt{2}\epsilon}d(\vec{r})\right)\right)\partial_j\partial_i d(\vec{r}) + \cdots \\ \cdots + 2\left(\frac{1}{\sqrt{2}\epsilon}\right)^2\left(-\tanh\left(\frac{1}{\sqrt{2}\epsilon}d(\vec{r})\right)+\tanh^3\left(\frac{1}{\sqrt{2}\epsilon}d(\vec{r})\right)\right)\partial_j d(\vec{r})\partial_i d(\vec{r}) \Leftrightarrow \\ \Leftrightarrow \partial_j\partial_i\phi = \frac{1}{\sqrt{2}\epsilon}\left(1-\phi^2\right)\partial_{ij}d(\vec{r}) + \frac{1}{\epsilon^2}\left(-\phi+\phi^3\right)\partial_i d(\vec{r})\partial_j d(\vec{r}) \end{gathered} \tag{A.24}$$

A.5.2 Integrating $(\nabla\phi)^2$

$$\int_{-\infty}^{\infty}\frac{1}{2\epsilon^2}\left(1-\phi^2\right)^2 dx = \int_{-\infty}^{\infty}\frac{1}{2\epsilon^2}\left(1-\tanh^2\left(\frac{1}{\sqrt{2}\epsilon}x\right)\right)^2 dx \tag{A.25}$$

Considering $u = \frac{x}{\sqrt{2}\epsilon}$ and $du = \frac{dx}{\sqrt{2}\epsilon}$

$$\int_{-\infty}^{\infty} \frac{\sqrt{2}\epsilon}{2\epsilon^2} \left(1 - \tanh^2(u)\right)^2 du \tag{A.26}$$

and further $v = \tanh(u)$ with $dv = \left(1 - \tanh^2(u)\right) du = \left(1 - v^2\right) du$, changing the limits from $]-\infty, \infty[$ to $]-1, 1[$

$$\begin{aligned} \int_{-1}^{1} \frac{\sqrt{2}}{2\epsilon\left(1-v^2\right)} \left(1-v^2\right)^2 dv = \int_{-1}^{1} \frac{\sqrt{2}}{2\epsilon} \left(1-v^2\right) dv = \\ = \frac{\sqrt{2}}{2\epsilon} \left[2 - \left(\frac{1^3}{3} - \frac{(-1)^3}{3}\right)\right] = \frac{2\sqrt{2}}{3\epsilon} \end{aligned} \tag{A.27}$$

A.5.3 Free Energy Functional Calculation

Note: As $\delta\phi$ is infinitesimal, all of the terms with its order equal or above 2 will be disregarded.

Considering only the bending energy:

$$\begin{aligned} E_b[\phi + \delta\phi] = \int k_1 \left(\phi + \delta\phi - (\phi + \delta\phi)^3 + \epsilon^2 \nabla^2 (\phi + \delta\phi)\right)^2 d\vec{r} = \\ = k_1 \int \left(\phi + \delta\phi - \left(\phi^3 + 3\phi^2\delta\phi + 3\phi\delta\phi^2 + \delta\phi^3\right) + \epsilon^2\nabla^2\phi + \epsilon^2\nabla^2\delta\phi\right)^2 d\vec{r} = \\ = k_1 \int \left(\left(\phi - \phi^3 + \epsilon^2\nabla^2\phi\right) + \left(\delta\phi - 3\phi^2\delta\phi + \epsilon^2\nabla^2\delta\phi\right)\right)^2 d\vec{r} = \\ = k_1 \int \left(\phi - \phi^3 + \epsilon^2\nabla^2\phi\right)^2 d\vec{r} + k_1 \int 2\left(\phi - \phi^3 + \epsilon^2\nabla^2\phi\right)\left(\delta\phi - 3\phi^2\delta\phi + \epsilon^2\nabla^2\delta\phi\right) d\vec{r} \Leftrightarrow \\ \Leftrightarrow \delta E_b = k_1 \int 2\left(\phi - \phi^3 + \epsilon^2\nabla^2\phi\right)\left(1 - 3\phi^2\right)\delta\phi d\vec{r} + k_1 \int 2\left(\phi - \phi^3 + \epsilon^2\nabla^2\phi\right)\epsilon^2\nabla^2\delta\phi d\vec{r}. \end{aligned} \tag{A.28}$$

The second term in the right part of the last equation can be easily solved into the type of expression intended by integrating by parts twice. The ending result for the bending energy of the membrane is

$$\begin{aligned} \delta E_b = \int 2k_1 \left(\left(\phi - \phi^3 + \epsilon^2\nabla^2\phi\right)\left(1 - 3\phi^2\right) + \epsilon^2\nabla^2\left(\phi - \phi^3 + \epsilon^2\nabla^2\phi\right)\right)\delta\phi d\vec{r} \Leftrightarrow \\ \Leftrightarrow \frac{\delta E_b}{\delta\phi} = 2k_1 \left[\left(\phi - \phi^3 + \epsilon^2\nabla^2\phi\right)\left(1 - 3\phi^2\right) + \epsilon^2\nabla^2\left(\phi - \phi^3 + \epsilon^2\nabla^2\phi\right)\right]. \end{aligned} \tag{A.29}$$

The applied forces energy is determined by:

$$\begin{aligned} E_f[\phi + \delta\phi] = k_2 \int \vec{r}\cdot\vec{F}\left(1 - (\phi + \delta\phi)^2\right)^2 d\vec{r} = \\ = k_2 \int \vec{r}\cdot\vec{F}\left(\left(1 - \phi^2\right) - 2\phi\delta\phi\right)^2 d\vec{r} = k_2 \int \vec{r}\cdot\vec{F}\left(\left(1-\phi^2\right)^2 - 4\left(1-\phi^2\right)\phi\delta\phi\right) d\vec{r} = \\ = k_2 \int \vec{r}\cdot\vec{F}\left(1-\phi^2\right)^2 d\vec{r} - 4k_2 \int \vec{r}\cdot\vec{F}\left(1-\phi^2\right)\phi\delta\phi d\vec{r} \Leftrightarrow \\ \Leftrightarrow \delta E_f = -4k_2 \int \vec{r}\cdot\vec{F}\left(1-\phi^2\right)\phi\delta\phi d\vec{r} \Leftrightarrow \frac{\delta E_f}{\delta\phi} = -4k_2(\vec{r}\cdot\vec{F})\left[\left(1-\phi^2\right)\phi\right]. \end{aligned} \tag{A.30}$$

Volume conservation term defined as:

$$\begin{aligned}
E_v[\phi+\delta\phi] &= -P\int \frac{(1+\phi+\delta\phi)^2}{4}(2-\phi-\delta\phi)d\vec{r} = \\
&= -P\int \frac{\left(1+\phi^2\right)^2+2\left(1+\phi\right)\delta\phi}{4}(2-\phi-\delta\phi)d\vec{r} = \\
= -P\int\left(\frac{1+\phi}{2}\right)^2(2-\phi)d\vec{r} &+ P\int\left(\frac{1+\phi}{2}\right)^2\delta\phi d\vec{r} - \frac{P}{2}\int(1+\phi)(2-\phi)\delta\phi d\vec{r} \Leftrightarrow \\
&\Leftrightarrow \delta E_v = -\frac{3}{4}P\int\left(1-\phi^2\right)\delta\phi d\vec{r} \Leftrightarrow \\
&\Leftrightarrow \frac{\delta E_v}{\delta\phi} = -\frac{3}{4}P\left(1-\phi^2\right).
\end{aligned} \tag{A.31}$$

And, finally, the surface area conservation term is obtained by

$$\begin{aligned}
E_s[\phi+\delta\phi] &= \sigma k_2\int\left(1-(\phi+\delta\phi)^2\right)^2 d\vec{r} = \sigma k_2\int\left(\left(1-\phi^2\right)-2\phi\delta\phi\right)^2 d\vec{r} = \\
&= \sigma k_2\int\left(\left(1-\phi^2\right)^2-4\phi\delta\phi\left(1-\phi^2\right)\right)d\vec{r} = \\
&= \sigma k_2\int\left(1-\phi^2\right)^2 d\vec{r} - 4\sigma k_2\int\phi\left(1-\phi^2\right)\delta\phi d\vec{r} \Leftrightarrow \\
&\Leftrightarrow \delta E_s = -4\sigma k_2\int\phi\left(1-\phi^2\right)\delta\phi d\vec{r} \Leftrightarrow \\
&\Leftrightarrow \frac{\delta E_s}{\delta\phi} = -4\sigma k_2\left[\left(1-\phi^2\right)\phi\right].
\end{aligned} \tag{A.32}$$

A.5.4 Volume and Surface Area Considerations

As the idea is to minimize the bending energy of the cell, and having into consideration that the spherical shape has the minimum value, the cell sides were chosen so as to accommodate the proportionality between both the surface area $A_{max} = 4\pi r^2$ and the maximum volume $V_{max} = \frac{4}{3}\pi r^3$:

$$V_{max} = \frac{1}{6}\left(\frac{A^3}{\pi}\right)^{\frac{1}{2}}. \tag{A.33}$$

It is important to note that cells are not spheres and therefore the volume chosen was smaller. Here, the selected volume fraction is 0.60. In other words, the initial volume is $V = 0.6V_{max}$

Considering the sides a, b, c of the parallelepiped region, its volume is $V = abc$ and the correspondent surface area is $A = 2(ac + bc + ab)$. Defining a as a predefined number and considering $c = \frac{V}{ab}$, b can be obtained by

$$\begin{aligned}
A = 2\frac{V}{b} + 2\frac{V}{a} + 2ab \Leftrightarrow Ab = 2V + 2\frac{Vb}{a} + 2ab^2 \Leftrightarrow \\
\Leftrightarrow b = \frac{\left(A-2\frac{V}{A}\right) \pm \sqrt{\left(A-2\frac{V}{a}\right)^2 - 16aV}}{4a}
\end{aligned} \tag{A.34}$$

subject to the constraint that $\left(A-2\frac{V}{a}\right)^2 - 16aV > 0$.

A.6 2D mRNA Transport Model

A.6.1 Applying PFM to the mRNA Equations

The first change is that the time derivative is not applied to m_f but to its product by ϕ

$$\frac{\partial}{\partial t} m_f \Phi = m_f \frac{\partial}{\partial t}\Phi + \Phi \frac{\partial}{\partial t} m_f. \tag{A.35}$$

However, as in this part of the model the order parameter is approximated to a constant field and, therefore, the first part of the right hand side is null.

$$\begin{aligned} \Phi \frac{\partial}{\partial t} m_f &= k_d \nabla^2 (m_f \Phi) - \lambda_f m_f \Phi - \gamma m_f \Phi \xi \left(\frac{M_m - m_l}{M_m} \right) + \frac{\beta_m (1-\xi) m_l}{\xi} \Leftrightarrow \\ \Leftrightarrow \frac{\partial}{\partial t} m_f &= \frac{k_d}{\Phi} \nabla^2 (m_f \Phi) - \lambda_f m_f - \gamma m_f \xi \left(\frac{M_m - m_l}{M_m} \right) + \frac{\beta_m (1-\xi) m_l}{\Phi \xi}. \end{aligned} \tag{A.36}$$

The equation for the concentration of linked mRNA is not affected in the same way as this mRNA does not depend on the order parameter. The only term to be influenced by Φ is the binding, i.e., when a fragment of the free mRNA links the MT, as this quantity is represented as $m_f \Phi$.

A.7 Euler Method

There are many ways to try to solve differential equations and are usually based off on the idea of finding the best approximation for the derivative of a function $x(t)$. This is found by using the Taylor expansion, as the first term $x(t_0)$ is already known

$$x(t + \Delta t) = x(t) + \frac{d}{dt} x(t) \Delta t + \frac{1}{2} \frac{d^2}{dt^2} x(t) \Delta t^2 + \frac{1}{6} \frac{d^3}{dt^3} x(t) \Delta t^3 + \cdots. \tag{A.37}$$

The Euler method is an explicit numerical algorithm to solve such differential equations. As it only considers the first order term of the series, it is a very simple model to implement, which usually is only recommended for simple implementations and exploratory work

$$x(t + \Delta t) = x(t) + \frac{d}{dt} x(t) \Delta t. \tag{A.38}$$

Please note, as the time step Δt in this type of algorithms is constant, it does not adapt to the necessity of more or less points throughout the time evolution of the system.

A.8 Mathematical Operators Implementation

As it can be seen throughout the equations of both models, there are some mathematical operators applied, namely different variations of the ∇ symbol. This represents a simple notation for the vector represented in the equation (A.1). In this work, it can either represent the gradient of a function (the result is a vector), the divergence of a vector (which is simply the scalar product and as such the result is a scalar) or as the scalar operator Laplacian, resulting

in the sum of the second partial derivatives of a function.

To implement these operators, they first have to be discretized. The best way to do so is by using the Taylor expansion for the function, so as to obtain a spacial definition for each value in a matrix. The expansions, representing only the first terms (second order discretization) as greater orders of the steps Δx and Δy can be considered insignificant, are:

$$\begin{aligned} f(i+1,j) &= f_{i,j} + \Delta x \frac{\partial f}{\partial x} + \frac{\Delta x^2}{2}\frac{\partial^2 f}{\partial x^2}, \\ f(i-1,j) &= f_{i,j} - \Delta x \frac{\partial f}{\partial x} + \frac{\Delta x^2}{2}\frac{\partial^2 f}{\partial x^2}, \\ f(i,j+1) &= f_{i,j} + \Delta y \frac{\partial f}{\partial y} + \frac{\Delta y^2}{2}\frac{\partial^2 f}{\partial y^2}, \\ f(i,j-1) &= f_{i,j} - \Delta y \frac{\partial f}{\partial y} + \frac{\Delta y^2}{2}\frac{\partial^2 f}{\partial y^2}. \end{aligned} \tag{A.39}$$

The idea is to sum the i and j variations (which, if infinitesimal are approximately the x and y derivatives) so as to obtain and isolate the differential terms needed. For example, applying the discretization to the Laplacion $\nabla^2 f = \frac{\partial^2 f}{\partial x^2} + \frac{\partial^2 f}{\partial y^2}$ works as such: from the sum of the two top equations in the aforementioned expression, the expression for $\frac{\partial^2 f}{\partial x^2}$ can be obtained and analogously for the bottom two. Assuming $\Delta x = \Delta y$, the intended Laplacian expression is:

$$\nabla^2 f = \frac{1}{\Delta x^2}\left(f(i+1,j) + f(i-1,j) + f(i,j+1) + f(i,j-1) - 4f(i,j)\right). \tag{A.40}$$

Which means that the Laplacian applied to each point (i,j) depends on its neighbours. Computationally, it is significantly easier to implement this notation to a discrete matrix. As the mathematical operators applied depend on the neighbours, it is important to guarantee that the changes are not influencing the current matrix, i.e., at any given iteration of the process, there are two separate matrices (one with the previously calculated values and the other with the values currently being computed) so as to guarantee that the new matrix will not be affected by the changes occurring at the current time step.

Bibliography

[1] S. T. Brady, G. J. Siegel, R. W. Albers, and D. L. Price, *Basic neurochemistry : Principles of molecular, cellular, and medical neurobiology*, 8th. Amsterdam ; Boston: Elsevier Academic Press, 2012, xxiv, 1096 p. ISBN: 9780123749475 0123749476.

[2] C. Conde and A. Caceres, "Microtubule assembly, organization and dynamics in axons and dendrites", *Nature Reviews Neuroscience*, vol. 10, no. 5, pp. 319–332, 2009, ISSN: 1471-0048.

[3] A. C. Rego and C. Pereira, *Support materials to neurobiology i and ii*, 2014.

[4] D. Purves, *Neuroscience*, 5th. Sunderland, MA: Sinauer Associates, 2012, xvi, 759, 60 p. ISBN: 9780878936953.

[5] E. D. Enger, F. C. Ross, and D. B. Bailey, *Concepts in biology*. McGraw Hill, 2008, Previous ed.: London: McGraw-Hill, 2006.

[6] C. E. Holt and E. M. Schuman, "The central dogma decentralized: New perspectives on rna function and local translation in neurons", *Neuron*, vol. 80, no. 3, pp. 648–657, 2013, ISSN: 0896-6273.

[7] H. Jung, C. G. Gkogkas, N. Sonenberg, and C. E. Holt, "Remote control of gene function by local translation", *Cell*, vol. 157, no. 1, pp. 26–40, 2014, ISSN: 0092-8674.

[8] B. C. Yoon, K. H. Zivraj, and C. E. Holt, "Local translation and mrna trafficking in axon pathfinding", *Results Probl Cell Differ*, vol. 48, pp. 269–88, 2009, ISSN: 0080-1844 (Print) 0080-1844 (Linking).

[9] D. S. Campbell and C. E. Holt, "Chemotropic responses of retinal growth cones mediated by rapid local protein synthesis and degradation", *Neuron*, vol. 32, no. 6, pp. 1013–1026, 2001, ISSN: 0896-6273.

[10] U. Hengst, A. Deglincerti, H. J. Kim, N. L. Jeon, and S. R. Jaffrey, "Axonal elongation triggered by stimulus-induced local translation of a polarity complex protein", *Nature Cell Biology*, vol. 11, no. 8, 1024–U263, 2009, ISSN: 1465-7392.

[11] C. E. Holt and S. L. Bullock, "Subcellular mrna localization in animal cells and why it matters", *Science*, vol. 326, no. 5957, pp. 1212–1216, 2009, ISSN: 0036-8075.

[12] A. M. Krichevsky and K. S. Kosik, "Neuronal rna granules: A link between rna localization and stimulation-dependent translation", *Neuron*, vol. 32, no. 4, pp. 683–696, 2001, ISSN: 0896-6273.

[13] B. C. Yoon, H. Jung, A. Dwivedy, C. M. O'Hare, K. H. Zivraj, and C. E. Holt, "Local translation of extranuclear lamin b promotes axon maintenance", *Cell*, vol. 148, no. 4, pp. 752–764, 2012, ISSN: 0092-8674.

[14] L. F. Gumy, C. L. Tan, and J. W. Fawcett, "The role of local protein synthesis and degradation in axon regeneration", *Experimental Neurology*, vol. 223, no. 1, pp. 28–37, 2010, ISSN: 0014-4886.

[15] S. Yoo, E. A. van Niekerk, T. T. Merianda, and J. L. Twiss, "Dynamics of axonal mrna transport and implications for peripheral nerve regeneration", *Experimental Neurology*, vol. 223, no. 1, pp. 19–27, 2010, ISSN: 0014-4886.

[16] L. I. Benowitz and Y. Q. Yin, "Combinatorial treatments for promoting axon regeneration in the cns: Strategies for overcoming inhibitory signals and activating neurons' intrinsic growth state", *Developmental Neurobiology*, vol. 67, no. 9, pp. 1148–1165, 2007, ISSN: 1932-8451.

[17] W. R. Holmes and L. Edelstein-Keshet, "A comparison of computational models for eukaryotic cell shape and motility", *Plos Computational Biology*, vol. 8, no. 12, 2012, ISSN: 1553-7358.

[18] J. K. Krottje and A. van Ooyen, "A mathematical framework for modeling axon guidance", *Bulletin of Mathematical Biology*, vol. 69, no. 1, pp. 3–31, 2007, ISSN: 0092-8240.

[19] T. Kobayashi, K. Terajima, M. Nozumi, M. Igarashi, and K. Akazawa, "A stochastic model of neuronal growth cone guidance regulated by multiple sensors", *Journal of Theoretical Biology*, vol. 266, no. 4, pp. 712–722, 2010, ISSN: 0022-5193.

[20] Y. E. Pearson, E. Castronovo, T. A. Lindsley, and D. A. Drew, "Mathematical modeling of axonal formation part i: Geometry", *Bulletin of Mathematical Biology*, vol. 73, no. 12, pp. 2837–2864, 2011, ISSN: 0092-8240.

[21] X. Descombes, E. Zhizhina, and S. Komech, "Modelling axon growing using ctrw", 2015.

[22] H. Nguyen, P. Dayan, Z. Pujic, J. Cooper-White, and G. J. Goodhill, "A mathematical model explains saturating axon guidance responses to molecular gradients", *Elife*, vol. 5, 2016, ISSN: 2050-084x.

[23] R. Costa, L. Macedo, J. Malva, and E. Costa, "Computational model of axon guidance", 2009.

[24] B. P. Graham and A. van Ooyen, "Mathematical modelling and numerical simulation of the morphological development of neurons", *Bmc Neuroscience*, vol. 7, 2006, ISSN: 1471-2202.

[25] T. Takaki, K. Nakagawa, Y. Morita, and E. Nakamachi, "Phase-field modeling for axonal extension of nerve cells", *Mechanical Engineering Journal*, 2015.

[26] G. J. Goodhill, R. A. Faville, D. J. Sutherland, B. A. Bicknell, A. W. Thompson, Z. Pujic, B. Sun, E. M. Kita, and E. K. Scott, "The dynamics of growth cone morphology", *Bmc Biology*, vol. 13, 2015, ISSN: 1741-7007.

[27] D. Y. Shao, H. Levine, and W. J. Rappel, "Coupling actin flow, adhesion, and morphology in a computational cell motility model", *Proceedings of the National Academy of Sciences of the United States of America*, vol. 109, no. 18, pp. 6851–6856, 2012, ISSN: 0027-8424.

[28] M. Naoz, U. Manor, H. Sakaguchi, B. Kachar, and N. S. Gov, "Protein localization by actin treadmilling and molecular motors regulates stereocilia shape and treadmilling rate", *Biophysical Journal*, vol. 95, no. 12, pp. 5706–5718, 2008, ISSN: 0006-3495.

[29] G. Orly, M. Naoz, and N. S. Gov, "Physical model for the geometry of actin-based cellular protrusions", *Biophysical Journal*, vol. 107, no. 3, pp. 576–587, 2014, ISSN: 0006-3495.

[30] K. S. Zadeh and S. B. Shah, "Mathematical modeling and parameter estimation of axonal cargo transport", *Journal of Computational Neuroscience*, vol. 28, no. 3, pp. 495–507, 2010, ISSN: 0929-5313.

[31] Z. Szymanska, M. Parisot, and M. Lachowicz, "Mathematical modeling of the intracellular protein dynamics: The importance of active transport along microtubules", *Journal of Theoretical Biology*, vol. 363, pp. 118–128, 2014, ISSN: 0022-5193.

[32] L. F. Gumy, E. A. Katrukha, L. C. Kapitein, and C. C. Hoogenraad, "New insights into mrna trafficking in axons", *Developmental Neurobiology*, vol. 74, no. 3, pp. 233–244, 2014, ISSN: 1932-8451.

[33] S. Najem and M. Grant, "Coupling actin dynamics to phase-field in modeling neural growth", *Soft Matter*, vol. 11, no. 22, pp. 4476–4480, 2015, ISSN: 1744-683x.

[34] S. Diehl, E. Henningsson, and A. Heyden, "Efficient simulations of tubulin-driven axonal growth", *J Comput Neurosci*, 2016, ISSN: 1573-6873 (Electronic) 0929-5313 (Linking).

[35] X. N. Chen and W. P. Zhu, "A mathematical model of regenerative axon growing along glial scar after spinal cord injury", *Computational and Mathematical Methods in Medicine*, 2016, ISSN: 1748-670x.

[36] N. Provatas and K. Elder, *Phase-field methods in materials science and engineering*, Electronic Book, 2010.

[37] M. E. S. Borelli, "Aspects of fluctuating membranes", Berlin, Freie Univ., Diss., 2000, 2000.

[38] F. Campelo and A. Hernandez-Machado, "Dynamic model and stationary shapes of fluid vesicles", *European Physical Journal E*, vol. 20, no. 1, pp. 37–45, 2006, ISSN: 1292-8941.

[39] I. Derenyi, F. Julicher, and J. Prost, "Formation and interaction of membrane tubes", *Physical Review Letters*, vol. 88, no. 23, 2002, ISSN: 0031-9007.

[40] R. D. M. Travasso, E. C. Poire, M. Castro, J. C. Rodrguez-Manzaneque, and A. Hernandez-Machado, "Tumor angiogenesis and vascular patterning: A mathematical model", *Plos One*, vol. 6, no. 5, 2011, ISSN: 1932-6203.

[41] J. Kockelkoren, H. Levine, and W. J. Rappel, "Computational approach for modeling intra- and extracellular dynamics", *Physical Review E*, vol. 68, no. 3, 2003, ISSN: 1539-3755.